SPECTRAL AND TEMPORAL FIDELITY OF A HARD X-RAY WEAPONS EFFECTS SIMULATION TEST IN A HIGH-GAIN ICF FACILITY

THESIS

Don F. Nichols
Second Lieutenant, USAF

AFIT/GNE/ENP/89M-6

DEPARTMENT OF THE AIR FORCE
AIR UNIVERSITY
AIR FORCE INSTITUTE OF TECHNOLOGY
Wright-Patterson Air Force Base, Ohio

AFIT/GNE/ENP/89M-6

SPECTRAL AND TEMPORAL FIDELITY OF A HARD X-RAY WEAPONS EFFECTS SIMULATION TEST IN A HIGH-GAIN ICF FACILITY

THESIS

Don F. Nichols
Second Lieutenant, USAF

AFIT/GNE/ENP/89M-6

Approved for public release; distribution unlimited

AFIT/GNE/ENP/89M-6

SPECTRAL AND TEMPORAL FIDELITY OF A HARD X-RAY WEAPONS EFFECTS SIMULATION TEST IN A HIGH-GAIN ICF FACILITY

THESIS

Presented to the Faculty of the School of Engineering
of the Air Force Institute of Technology
Air University
In Partial Fulfillment of the
Requirements for the Degree of
Master of Science in Nuclear Engineering

Don F. Nichols, B.S.
Second Lieutenant, USAF

March 1989

Approved for public release; distribution unlimited.

Preface

The effectiveness of our nuclear arsenal to act as a nuclear deterrent hinges in part upon the credibility of its survivability. Simply stated, if a potential adversary does not believe our arsenal would survive deployment during a nuclear exchange then our weapons present a reduced threat to him. To ensure the survivability of our nuclear weaponry, we must be able to test critical systems and components in environments that realistically simulate the stresses created by a nuclear environment. Currently, there are serious gaps in our weapons effects simulations capabilities; should a comprehensive nuclear test ban treaty be signed, these gaps would become even more severe.

This work examined the feasibility of using the hard X-ray pulse generated in the proposed Laboratory Microfusion Facility (LMF) for hard X-ray weapons effects simulation. The construction of the LMF is a necessary next step in the development of inertial confinement fusion power for commercial electricity generation; the application of the LMF to weapons effects testing could significantly enhance the national security. The increased funding resulting from weapons effects applications would encourage the development and construction of the LMF and thereby encourage the development of nuclear power for peaceful purposes.

There are a number of people who provided help and valuable guidance to me on this project. Captain Mike Tobin, my sponsor from LLNL, provided much of the background information used in this work and his enthusiasm for the project was contagious. Major Denis Beller, my advisor from AFIT, was always willing to talk with me when I arrived (usually without an appointment) at his door, bursting to share something new I had learned. He was also especially helpful in sorting out problems with the computer code and in providing general guidance and direction to the work. My wife, Kathy, and my children, Jason, Mark and Hannah, supported me through what was a difficult time for all of us; I cherish them deeply and am thankful for such a wonderful family. More than anyone else, however, I would like to express my gratitude to my Lord Jesus Christ, who is my breath, and who was the real reason I came to AFIT in the first place.

Don F. Nichols

March 6, 1989

Contents

List of Figures

List of Tables

Abstract

This work examined the feasibility of using the proposed Laboratory Microfusion Facility (LMF) to simulate the effects of hard X rays from a nuclear weapon. The LMF will be an inertial confinement fusion facility for the testing of high-gain deuterium-tritium (DT) pellets, and will produce a pulse of hard X rays and neutrons over a very short time interval. The purpose of the study was to determine (1) the intensity that remains after the X-ray pulse is stretched to the 10's of ns required for weapons effects work, (2) the effects of the temporal stretching on the final X-ray spectrum, and (3) the intensity of the neutron fluence and neutron-generated gamma rays. Using the MORSE-CG Monte Carlo code, a spherical shell of ^{6}LiH with a thickness of 60 cm was found to spread an instantaneous 10 keV X-ray pulse temporally over a period of 16 ns. The spectrum of the resultant X-ray pulse was somewhat softer than that of the input spectrum; the 10 keV input X-ray spectrum was peaked at 37.5 keV while the final spectrum was peaked at 25 keV. Eighty-seven percent of the X-ray energy fluence was lost to the LiH, resulting in a final fluence of 10.8 cal/cm^2 and a final dose of 9.3 Mrads(Si) 250 cm from the source. Fifty percent of the X-ray dose arrived during an interval of 6 ns, giving a dose rate of $8*10^{14}$ rads(Si)/sec. The only serious problem with the use of the LMF for hard X-ray simulation was the fluence of one-MeV-

equivalent neutrons. The minimum fluence was on the order of $1*10^{14}$ n/cm^2, but preliminary work has indicated that this value could be reduced by an appropriate shadow shield.

SPECTRAL AND TEMPORAL FIDELITY OF A HARD X-RAY WEAPONS EFFECTS SIMULATION TEST IN A HIGH-GAIN ICF FACILITY

I. Introduction

Background

In the design of weapons systems it is essential that the weapons designer be able to assess not only the lethality of his weapon, but also its vulnerability to real-world threat environments. A weapon is only as good as its ability to survive its journey to the target; if, for example, a re-entry vehicle is rendered impotent by the effects of a precursor nuclear burst, it has been launched in vain. For this reason, an entire scientific community has evolved around the work of weapons vulnerability, lethality and effects (VLE). This community has spent considerable time and effort developing simulators that attempt to re-create the radiation effects which weapons systems would experience during a nuclear exchange. Such simulation is quite a task, as the nuclear environment produces a complex set of synergistic phenomena through the interaction of X rays, gamma rays, neutrons and weapons debris with the weapon system. Adequate simulation of the nuclear

environment requires special attention to the spectral and temporal characteristics of the actual stockpile-to-target threat sequence (STS); the degree to which a particular simulator duplicates the stresses produced by these characteristics is known as the fidelity of the simulator.

While an examination of all the effects of a nuclear detonation is outside the scope of this paper, the problem of weapons effects simulation can be illuminated by a brief examination of some of the principal photon and neutron effects that must be considered in weapons effects simulation.

Photon Effects. The X-ray flux from an endo-atmospheric nuclear burst is quickly absorbed by the atmosphere, and its effect on other weapons systems is usually only of minor importance. The X-ray flux from an exo-atmospheric nuclear burst is diminished only by spherical divergence, however, and large X-ray fluences can be present at great distances from the burst. These X rays can seriously affect vehicles, such as satellites and re-entry vehicles (RV's), that move outside the earth's atmosphere. High fluences of low-energy X rays on the surface of a RV can ablate its heat shield. If the shield is sufficiently damaged it may not provide adequate protection and the RV may burn up during re-

entry into the atmosphere. Large doses of low-energy X rays over short time scales can give rise to a thermo-mechanical-shock response that propagates through the structural material and destroys the vehicle by spallation of internal surfaces(1:5.1,22). X and gamma rays can also dislodge electrons by the photoelectric effect. These electrons, if generated over a sufficiently short time and in sufficient quantity, can give rise to electric currents that interact to create a system generated electromagnetic pulse (SGEMP). This pulse can disrupt the internal electronics and lead to total system failure. Similarly, hard X and gamma rays can interact directly with the electronics and generate electrons through photoelectric and Compton interactions, and by pair production. In the semiconductors used in modern electronics, the electrons knocked free and the "holes" where they once resided can seriously change the characteristics of the affected device, causing changes in device states (upset) and voltage thresholds. High dose rates can result in the generation of large photocurrents that can destroy a device or burn out an entire circuit(2:275-296).

Neutron Effects. Neutrons can interact with the fissile material in a nuclear warhead and generate enough heat to asymmetrically soften its components, preventing a symmetric final compression and causing the

warhead to fail. Neutrons can also interact with the lattice structure of the semiconductors used in modern electronics to create defects that increase the resistivity of the semiconductor and reduce the minority carrier lifetime. This changes the device operating characteristics and may render affected devices and the components of which they are a part inoperable(3:385).

The neutron and photon effects presented above generate complex interactions between electronic devices at both the component and the system level. For this reason, it is desirable to test the effects of a species of radiation on an entire system, not just its components. Current above-ground test (AGT) X-ray simulation facilities are not adequate to test large items such as re-entry vehicles and satellites. Further, simultaneously achieving high fidelity with respect to X-ray spectrum, dose, dose rate and the rate with which the dose rate changes is quite difficult in AGT's and, perhaps surprisingly, even in underground tests (UGT's) using actual nuclear devices.

In view of this difficulty, the development of high-fidelity X-ray weapons effects simulators is of great importance to assuring the survivability of our nuclear weaponry and, therefore, of great importance to our national security. One facility currently being

evaluated for its weapons effects simulation capabilities is the Laboratory Microfusion Facility (LMF), a proposed facility to be used to test and develop high-gain inertial confinement fusion (ICF) pellet designs. Recent advances in the ICF field have led to the possibility of ICF pellets that could generate energy gains of 100 fold. The most promising pellet designs are those that use deuterium and tritium (DT) as the fusion fuel. These high-gain designs are predicted to be able to produce an energy pulse of 1 GJ for a 10 MJ driver at a power of 10^{17} to 10^{18} watts. This pulse will consist of a large neutron component and an X-ray component that, if it can be suitably tailored, could be used to simulate the hard X-ray pulse (X-ray energies greater than 10 keV) a device or weapons system might experience in space from a nuclear burst. The size of the facility and the amount of hard X-ray energy released by the fusion of the ICF pellet could make the LMF suitable for the hard X-ray testing of entire systems such as satellites or re-entry vehicles(4:5).

Problem and Scope

Several issues arise in regard to tailoring an ICF X-ray pulse for use in hard X-ray VLE simulation. The first issue to be resolved is the degree to which a pulse of X rays can be stretched temporally without sacrificing an acceptable dose outside the scattering medium. The ICF pulse is very short but Bridgman suggests that an exo-atmospheric X-ray pulse would be as long as several tens of nanoseconds(1:5.22). Substantial temporal stretching of the initial X-ray pulse would be required to achieve dose-rate fidelity; in the process the pulse could be substantially attenuated. To be attractive for hard X-ray simulation a dose greater than 1 Mrad(Si) must remain after the pulse has been lengthened. The second issue to be considered is the effect of the scattering process on the X-ray spectrum. In most materials, the absorption cross section for low-energy photons is much greater than for high-energy photons; the spectrum of an X-ray pulse passing through a material is typically hardened. Excessive pulse hardening could render the LMF unsuitable for VLE work. The final issue to be addressed is the neutron and neutron-generated gamma-ray fluence outside the scattering shell. High-energy neutrons can be a source of radiation damage to both structures and electronics. Neutron fluences greater

than 10^{13} MeV-equivalent neutrons/cm^2 would interfere with the X-ray effects being studied. The effects of a pulse of high-energy neutron-generated gamma rays could overwhelm the X-ray effects and deliver an unacceptably high total dose to electronics.

To resolve the issues raised above, the MORSE-CG Monte Carlo computer code was used to calculate hard X-ray and neutron doses outside a lithium hydride (LiH) shell in an LMF chamber. Lithium hydride was chosen as a scattering medium because of it's high scatter-to-absorption cross-section ratio for photons. The problem approach is presented in the following section.

Approach

The effects of various blankets of LiH on the ICF pulse were studied using the Multi-group Oak Ridge Stochastic Experiment - Combinatorial Geometry (MORSE-CG) computer code, distributed by the Radiation Shielding Information Center (RSIC) at Oak Ridge National Laboratory (ORNL). The steps to the investigation were as follows:

1. Compile and run the sample problems and code as supplied by RSIC, and fix any bugs discovered.

2. Premix cross-section data required by the specific problem, using the MORSE module XCHECKER.

3. Develop a simple geometry (using the MORSE module PICTURE) with which to check user-written routines.

4. Develop user-written routines to provide the specific source and detector responses required by the specific problem of interest.

5. Test the user-written routines using single group input spectrum and simple geometries.

6. Develop the specific geometry to be used for the actual problem and test it thoroughly using the MORSE module PICTURE.

7. Develop input spectral data for both X rays and neutrons, gamma-generation information (from the XCHECKER run), and any KERMA (Kinetic Energy Released in Material) factors desired. Combine these data with the geometry data to create the MORSE input file.

8. Run the problem and examine the results. Alter the geometry and rerun the problem to investigate relevant phenomena.

Of the above steps, steps one, three, four and five were actually preparatory steps, and are not the subject of this thesis. They did, however, consume an enormous amount of time. The routines developed in step four and the data developed in the remaining steps will be discussed in full in the body and appendices of this report.

Organization of Presentation

A detailed description of this investigation is presented in the chapters that follow. Chapter 2 presents background information on the MORSE code and briefly discusses the theory on which it operates. Chapter 2 also presents a brief discussion of the user-written routines and the geometry, cross-section and KERMA data. A large number of problems were run and analyzed in this work; Chapter 3 presents several selected problems, the results and discussion of which are illustrative of the major findings of this work. For clarity, each problem is discussed as it is presented. Chapter 4 presents the conclusions drawn from this work and gives specific recommendations for future work. A discussion of the functions of each of the user-written routines is presented along with their

source code in Appendix A and, finally, a sample data file is presented in Appendix B.

II. The MORSE Code

Description of the Code

Theory and Operation. The Multi-group Oak Ridge Stochastic Experiment - Combinatorial Geometry (MORSE-CG) computer code is a statistical approach to solving the Boltzman transport equation for both photons and neutrons. The code is based on an interpretation of the macroscopic cross section in which the cross section for a given nuclear reaction represents the probability per unit path length of that reaction occurring. A thorough discussion of the mechanics of the code would consume many volumes and is beyond the scope of this paper; a brief overview of the code is presented, however, in the following paragraphs.

The MORSE code is a multi-group, Monte Carlo code; the particle energy distribution is divided into user-defined groups (or bins), and the angular distribution is represented by an expansion of Legendre polynomials up to the sixteenth order (only a third order (P3) expansion was used in the calculations performed for this work). A simple text file is used to enter specific problem data. This file contains the multi-group source spectrum, its energy structure, the problem geometry and cross-section information. The source

spectrum is simply a listing of the number of source particles in each of the user-defined bins. For a coupled, neutron-photon calculation, the upper bins (which begin with bin number 1) of the source spectrum contain the neutron data and the lower bins contain the photon data. The code reads the spectral data from the input file, normalizes the total number of particles in the spectrum to 1, and uses the normalized spectrum to generate a batch of particles with the same spectral composition as the input spectrum. Each of these particles is assigned an initial direction, weight and velocity, based on the energy of the particle and various other parameters supplied by the user. Each particle is then "tracked" as it travels through and collides with the media which comprise the problem geometry.

At each collision site, particles can undergo a number of events. Particles can scatter into a new direction and/or into a new energy group, and may generate new particles through such mechanisms as pair production, neutron capture, or (n,2n) reactions. MORSE determines what happens at each collision through the use of cross sections, probabilities and random numbers. MORSE determines the chronological age of each particle by maintaining a running sum of the distance between collisions and boundary crossings, divided by the

particle speed. Particles are never absorbed in MORSE; at each collision site the pre-collision weight of the particle is reduced by the ratio of the cross section for absorption to the total cross section. This prevents absorption from decreasing the number of particles in the system and reduces the average contribution that single particles make to the total fluence at the detector, hence improving the statistics. Particles are tracked through the system until their weights become very small or they escape across the outer boundary of the geometry.

Eventually, a particle's weight becomes so small that the particle can no longer make a significant contribution to the total fluence. To continue to track such a particle only uses up computer time and does not move any closer to the solution of the original problem. To avoid tracking numerous particles with tiny weights, methods are available for 'combining' several low-weight particles to form a single particle, the weight of which equals the combined weights of the particles eliminated. This work used a method known as "Russian roulette". In Russian roulette, when a collided particle's weight falls below a user specified weight cutoff, the ratio of the current particle weight to a user-supplied survival weight is compared to a random number generated by the computer. If the random number is greater than the

ratio, the particle is killed and its history is terminated. If the random number is less than or equal to the ratio, the particle is given the user-supplied survival weight and allowed to continue(5:4-1,2,4-10,11).

The User-written Routines

The MORSE code is a system of subroutines called by a main program module. Standard subroutines included in the package perform functions that are common to all applications (such as the random walk process and statistical bookkeeping), but the user is expected to generate problem-specific routines. The routines to be generated for this work were the main routine (that calls MORSE), and subroutines named Bankr, Direc, Gtmed, Relcol, Sgam, Sdata, and Source. These routines were adapted from routines that already existed; the functions of these routines and their source code are presented in Appendix A.

Input Geometry Descriptions

An aluminum shell, 1 meter in thickness and with an inside radius of 5 meters, was used to simulate the LMF chamber. This shell, with it s contents, is illustrated in Figure 2.1, which is a compressed output from the MORSE module PICTURE. The chamber is surrounded by free space.

A pyrolytic-graphite cone with a height of two meters and a base radius of twenty-five centimeters was used to simulate a generic RV. It is illustrated in Figure 2.2. It is mounted to the wall of the chamber by two aluminum support cylinders, each five centimeters in radius. To maximize the uniformity of the X-ray fluence on the edge of the graphite cone nearest the source, the cone is positioned with the surface closest to the center of the chamber parallel to the vertical (or 'z') axis of the chamber (see Figure 2.1) and such that the 'x' axis of the chamber intersects the midpoint of the cone. To simulate semiconductor material in an aluminum casing inside an RV, a spherical silicon shell with an outer radius of 2.5 cm, an inner radius of 1.1 cm and a 0.254 cm casing of aluminum is located 1.25 cm inside the surface of the graphite cone closest to the source.

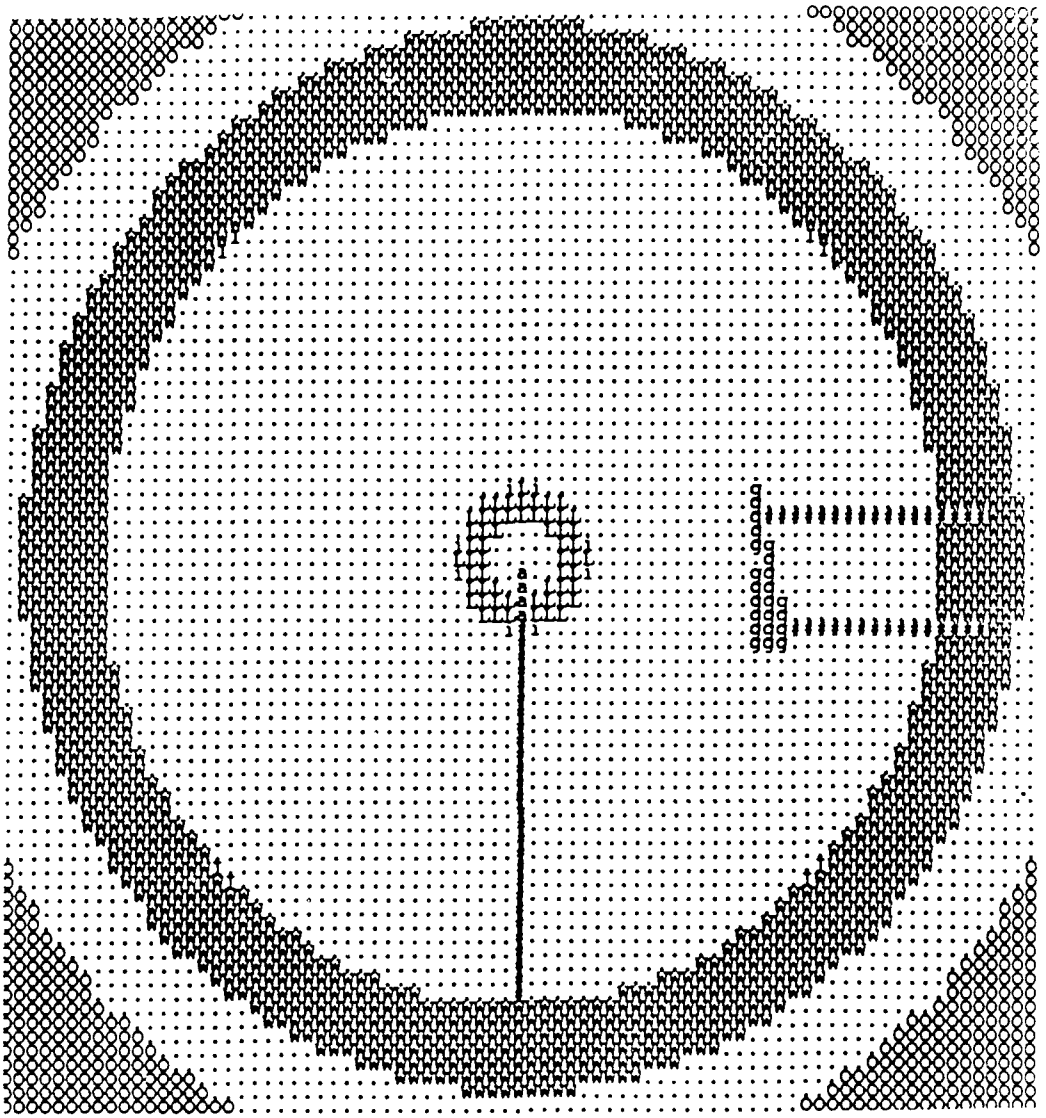

Note: Letters represent materials; g is graphite, L is Lithium hydride, W and # are aluminum, and . and O are free space. The chamber radius is 5 meters.

Figure 2.1: Basic Target Chamber Geometry

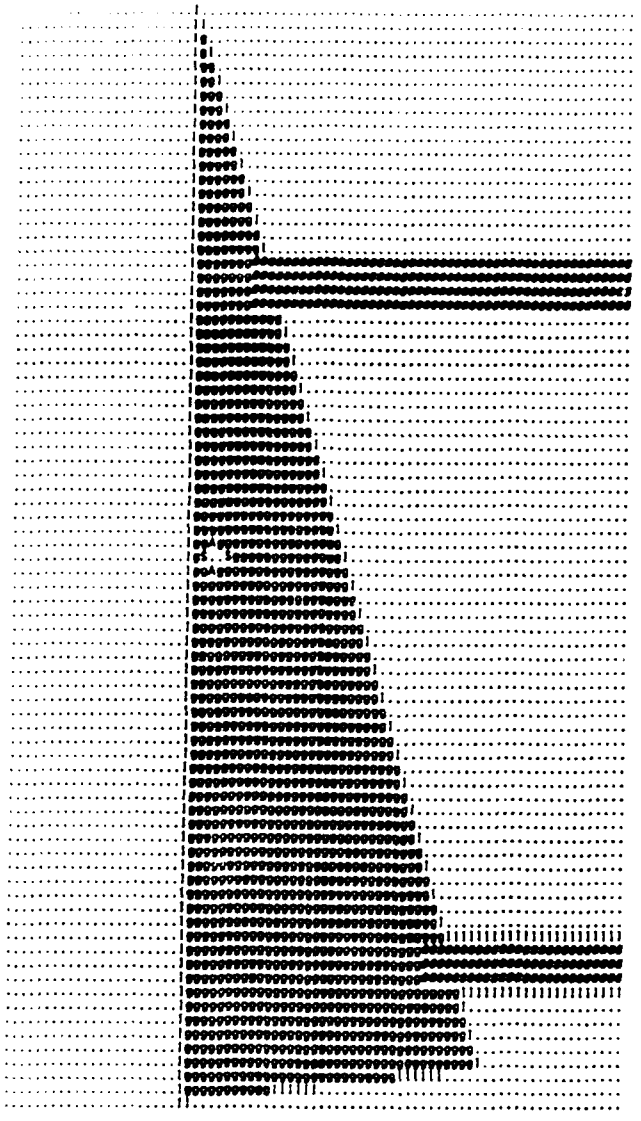

Note: Letters represent materials; g is graphite, # is aluminum, I is ice and . represents free space. The RV is 2 m in height with a base diameter of 50 cm.

Figure 2.2: Generic Conical Re-entry Vehicle

A shell of lithium hydride (LiH) was chosen to temporally stretch the X-ray pulse length and attenuate the neutron fluence. The PICTURE depiction of this shell is presented in Figure 2.3. The shell is located at the center of the LMF chamber, concentric to the

location of the source. The inner radius of the basic shell is 40 cm and the outer radius is 80 cm. It is supported by an aluminum pedestal five centimeters in radius. The ICF pellet would initially be supported by a stem; this was modeled using a tapered aluminum stem which extends through the LiH shell from the pedestal and ends five centimeters from the center of the chamber.

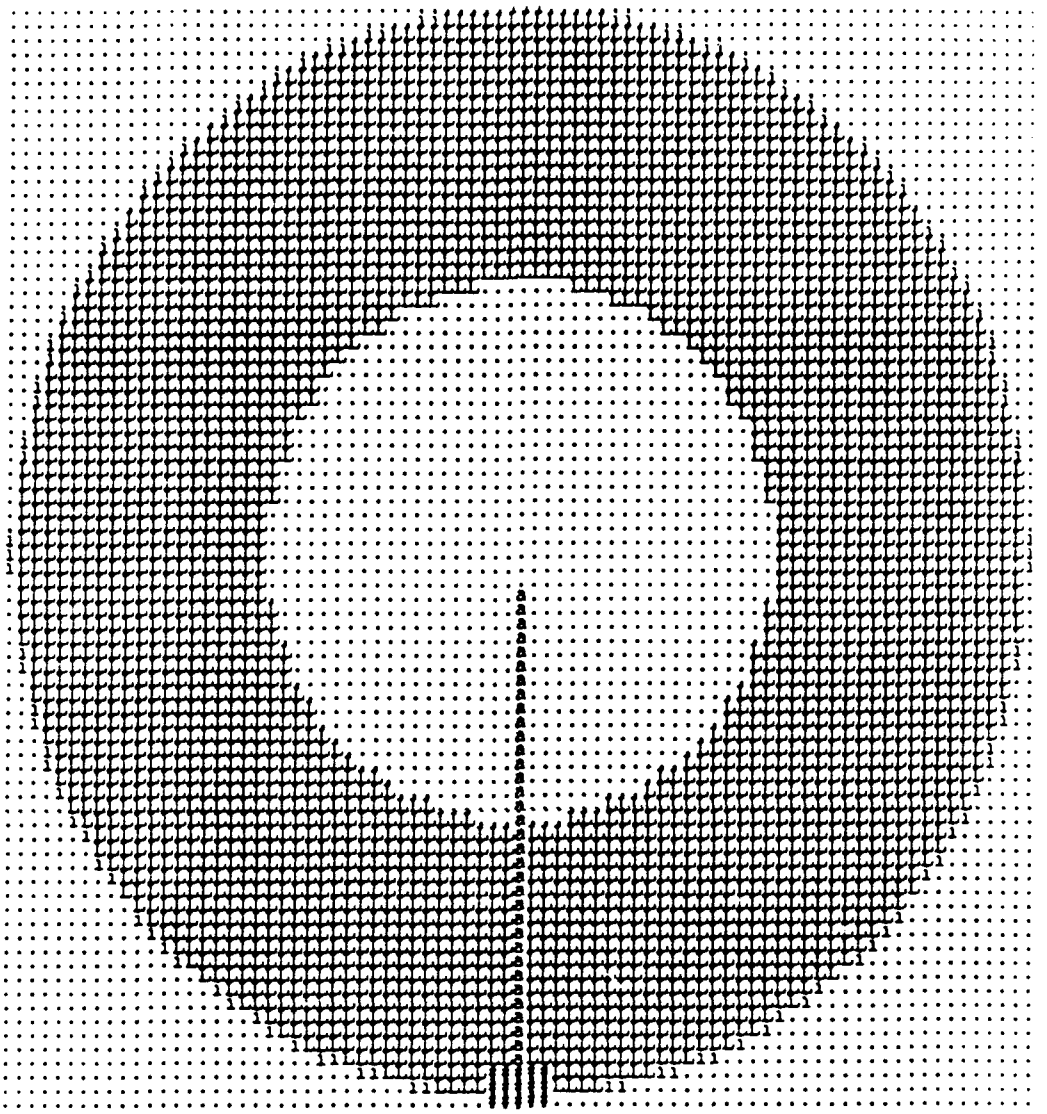

Note: Letters represent materials; L is lithium hydride, # is aluminum, i is ice and . represents free space. The inner radius is 40 cm and the outer radius is 80 cm.

Figure 2.3: The LiH Moderating Blanket

All surfaces outside the LiH shell and inside the aluminum chamber are coated with a layer of low density ice with a thickness of 1 cm. Each structure, such as the graphite cone, the wall, or the LiH shell can be

'turned off' for a given problem by setting its medium number in the data input file to 1000, the number signifying an internal void. A structure is 'turned on' by setting its medium number to the number representing the cross sections to be used for the structure. In this fashion the effects of the various chamber components can be examined separately or in combination.

The Input Spectrum

Since the actual output spectrum from an ICF capsule is classified, an actual spectrum was not used in this work. However, Chen(6:14) states that for a deuterium-tritium (DT) reaction, a plasma is required with a temperature in the 10 keV range. Thus, the X-ray spectrum used in this work is a 10 keV Planckian blackbody distribution. The distribution of neutrons with energy is presented in Table 2.1 and shown graphically in Figure 2.4. According to Friedlander et. al.(7:546), the neutrons produced in the DT reaction carry an average of 14.1 MeV of the 17.6 MeV released in the reaction, so the neutron spectrum used in this work is composed of predominantly 14 MeV neutrons with a lower-energy tail to account for neutrons which collide in the DT pellet.

Table 2.1: Neutron Distribution with Energy

Energy Range (MeV)	Neutrons in Range (% Total)
14-10	49.8
10-1	39.3
<1	10.9

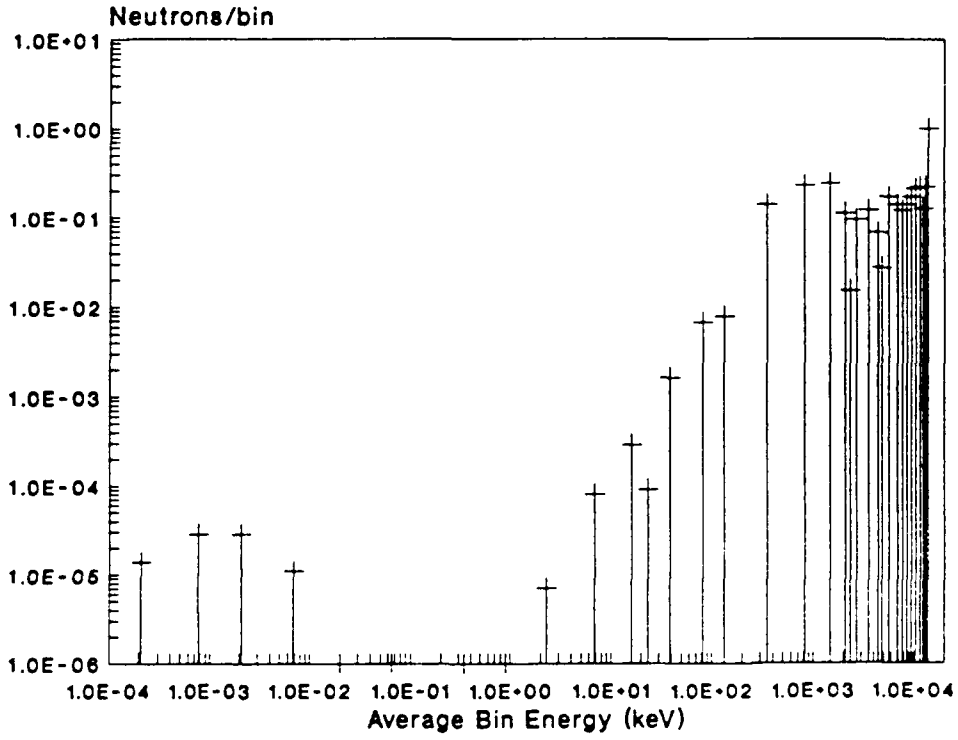

Figure 2.4: The Input Neutron Number Spectrum

Cross-section Data

The microscopic cross sections used in this work were supplied by RSIC at ORNL as a part of the FEWG1 RSIC Data Library Collection(8:1). This library supplies cross-section data for neutrons with energies from 10 micro-eV to 19.6 MeV and for photons with energies from 10 keV to 14 MeV. This range of photon cross sections limited this work to calculations with hard X rays. The material densities used to generate the macroscopic cross-sections are listed in Table 2.2.

Table 2.2: Materials and Densities

Material	Density gm/cc	atoms/b-cm
Aluminum	2.7	6.022E-2
LiH	0.6	4.520E-2
Graphite	2.2	1.104E-2
Ice	0.1	
Hydrogen		3.346E-3
Oxygen		6.691E-3
Boron	2.30	1.281E-1
In LiH	0.23	1.281E-2
Silicon	2.33	4.996E-2
Lead	11.3	3.284E-2

Detector Response Functions

The basic MORSE code produces fluence output in terms of particles per square centimeter per source particle. Because energy fluences were desired, the basic code was modified to give the fluence in terms of eV/cm^2/source particle. In many situations, however, it is not the raw fluence that is of interest, but rather the energy deposited in the material. Conveniently, the FEWG1 cross-section library used in this work also includes a set of KERMA (Kinetic Energy Released in MAterial) factors. The units on these factors are (rads-barn-gram)/(particle-atom) where 'particle' refers to the incident particle (neutron or photon) and 'atom' refers to the media on which the particle is impingent. To convert these units to rads/(eV/cm^2) it is necessary to divide the KERMA factor for each energy bin by the average bin energy in eV and by the atomic weight in grams and to then multiply by $10^{-24}cm^2$/barn.

The factors discussed above are convenient for X-ray and gamma-ray doses, but neutron fluences are typically reported in terms of one-MeV-equivalent neutrons/cm^2 (2:379,380). For a given fluence of neutrons with energy in dE about E, the one-MeV-equivalent fluence is defined as the fluence multiplied by the ratio of the KERMA factor for that energy divided by the KERMA factor

for a 1 MeV neutron, which Messenger gives for silicon as $1.52*10^{-9}$ Rads-barn-gram/particle-atom.

Using these values, response functions were calculated for use with the MORSE code. These function values are presented in Tables 2.3 and 2.4.

Table 2.3: Photon Detector Response Functions

Upper Energy Boundary (eV)	Output Units per Source Particle		
	eV/cm^2	rads(C) $(*10^{17})$	rads(Si) $(*10^{17})$
Energy	Response Function Values		
+1.4000 +7	1.	2.190 *	30.12
1.0000 +7	1.	2.331	29.76
8.0000 +6	1.	2.435	29.64
7.0000 +6	1.	2.540	29.91
6.0000 +6	1.	2.682	30.56
5.0000 +6	1.	2.870	31.52
4.0000 +6	1.	3.126	33.01
3.0000 +6	1.	3.392	34.85
2.5000 +6	1.	3.624	36.69
2.0000 +6	1.	3.914	39.22
1.5000 +6	1.	4.267	42.59
1.0000 +6	1.	4.581	45.74
7.0000 +5	1.	4.733	47.40
4.5000 +5	1.	4.698	47.53
3.0000 +5	1.	4.369	46.92
1.5000 +5	1.	3.698	55.79
1.0000 +5	1.	3.390	92.25
7.0000 +4	1.	3.453	241.9
4.5000 +4	1.	10.43	924.2
3.0000 +4	1.	16.35	3305.0
2.0000 +4	1.	92.77	17630.0

* Read as $2.19*10^{-17}$ + Read as $1.4*10^{7}$ eV

Table 2.4: Neutron Detector Response Functions

Upper Energy Boundary	Output Units per Source Particle		
	n^*/cm^2	rads(C)	rads(Si)
Energy(eV)	Response Function Values		
1.9600 +7[+]	3.208 -06	1.216 -17	1.047 -16
1.6900 +7	3.429 -06	1.186 -17	1.119 -16
1.4900 +7	3.543 -06	1.131 -17	1.156 -16
1.4200 +7	3.553 -06	1.167 -17	1.16 -16
1.3800 +7	3.490 -06	1.156 -17	1.139 -16
1.2800 +7	3.396 -06	1.182 -17	1.108 -16
1.2200 +7	3.254 -06	1.100 -17	1.062 -16
1.1100 +7	3.059 -06	1.130 -17	9.983 -17
1.0000 +7	2.828 -06	1.549 -17	9.229 -17
9.0500 +6	2.831 -06	9.79 -18	9.239 -17
8.1900 +6	3.070 -06	1.506 -17	1.002 -16
7.4100 +6	2.093 -06	6.93 -18	6.831 -17
6.3800 +6	1.155 -06	1.055 -17	3.770 -17
4.9700 +6	1.156 -06	1.068 -17	3.771 -17
4.7200 +6	9.899 -07	1.442 -17	3.230 -17
4.0700 +6	9.161 -07	2.472 -17	2.990 -17
3.0100 +6	1.136 -06	2.212 -17	3.706 -17
2.3900 +6	1.082 -06	1.830 -17	3.532 -17
2.3100 +6	1.403 -06	1.954 -17	4.579 -17
1.8300 +6	1.362 -06	2.180 -17	4.435 -17
1.1100 +6	1.838 -06	2.903 -17	5.999 -17
5.5000 +5	2.728 -06	3.643 -17	8.903 -17
1.5800 +5	4.078 -07	4.794 -17	1.331 -17
1.1100 +5	1.051 -06	4.844 -17	3.428 -17
5.2500 +4	0.000	5.019 -17	3.190 -17
2.4800 +4	0.000	5.313 -17	3.387 -17
2.1900 +4	0.000	5.121 -17	3.661 -17
1.0300 +4	0.000	4.906 -17	4.367 -17
3.3500 +3	0.000	5.018 -17	4.585 -17
1.2300 +3	0.000	5.196 -17	4.778 -17
5.8300 +2	0.000	4.370 -17	4.217 -17
1.0100 +2	0.000	4.841 -17	7.061 -17
2.9000 +1	0.000	4.674 -17	1.984 -16
1.0700 +1	0.000	5.090 -17	8.182 -16
3.0600 +0	0.000	6.606 -17	4.488 -15
1.1300 +0	0.000	1.208 -16	1.994 -14
4.1400 -1	0.000	1.093 -15	3.054 -13

[+] Read as $1.96*10^7$ eV * one-Mev-equivalent

III. Results

Organization

This chapter presents a selection of the results of this investigation. These results illustrate the significant information gained from the rather large number of problems run. For clarity, the problems presented are arranged by the nature of the information they contain and not necessarily in the order in which they were run. Further, to provide a clear and logical development of the conclusions of this work, each problem is discussed as the data pertaining to that problem are presented.

Dolan suggests an X ray energy fraction of 2 to 15 percent of a total yield of 30 to 3000 MJ(9:515). This work used a total energy output (ignoring debris) of 1000 MJ, and allocated 867 MJ as neutron source energy and 133 MJ as X-ray energy. This arbitrary energy distribution is used to give the order of magnitude of the effects being discussed.

The results are presented according to outline presented on the following page.

- X-ray Results (source neutrons off)

  LiH Shell in an LMF Chamber

- Neutron Results (source X rays off)

  LiH Shell in an LMF Chamber

- Combined (source X rays plus neutrons) Results

  LiH Shell in an LMF Chamber

  Dose in Rads(Carbon) and Rads(Silicon)
  at a Graphite Cone

- Reduction of Neutron and Gamma-ray Fluence

  Addition of Boron-10 to LiH

  Shielding of Wall Pulse

  Substitution of ^{6}LiH and Realistic Walls

X-ray Fluence, Dose and Arrival Times

The first issue of concern is the effect of the LiH scatterer on the total fluence and dose of hard X rays. To resolve this issue, a series of calculations was performed using only the X-ray portion of the input spectrum (i.e. with the neutrons turned 'off'). The temporal effects were restricted to those of the LiH shell and the chamber wall by turning all other material in the problem "off". Since the time interval over which the actual ICF X-ray pulse would be emitted from the DT capsule is very short compared to the length to which it must be stretched, the X-ray source was modeled as an instantaneous point source located at the center of the chamber. The X-ray energy fluence and dose as a function of time and LiH shell thickness are presented graphically in Figure 3.1 and numerically in Table 3.1. Note that although the information presented in Figure 3.1 and in the figures to follow is presented in the form of line graphs, the data are more accurately displayed in the form of a histogram. Each point actually represents the midpoint value of an energy or time bin; line graphs are used to clarify the interpretation of overlaid plots.

Table 3.1: Variation in X-Ray Fluence, Dose and Arrival Interval with ^{7}LiH Thickness

Outer radius (cm)	LiH Shell (cm)	Fluence (cal/cm^2)	Dose MRads(Si)	T50 (ns)	T90 (ns)
40	00	80 (1)	72 (2)	<1	<1
50	10	58.1(.5)	54.2(1)	<1	4(.5)
60	20	46.0(3)	39.7(1)	<1	5.2(1)
70	30	28.4(.8)	23.6(1)	1.5(.5)	7.3(1)
80	40	17.7(2)	15.6(1)	2.6(.5)	8 (1)
90	50	12.6(.7)	11.4(.8)	3.7(.5)	8.5(1)
100	60	8 (1)	7.3(.9)	4.4(1)	11 (2)

Note: Detector was located at 250 cm in free space. Neutrons were turned 'off' in these runs. Numbers in brackets are the standard deviations of the values they follow. T50 and T90 are the time intervals over which the first 50% and 90% (respectively) of the Dose arrives.

In the calculations presented in Table 3.1, the inner radius of the LiH shell was held fixed, so that increasing the thickness of the LiH shell also increased the diameter.

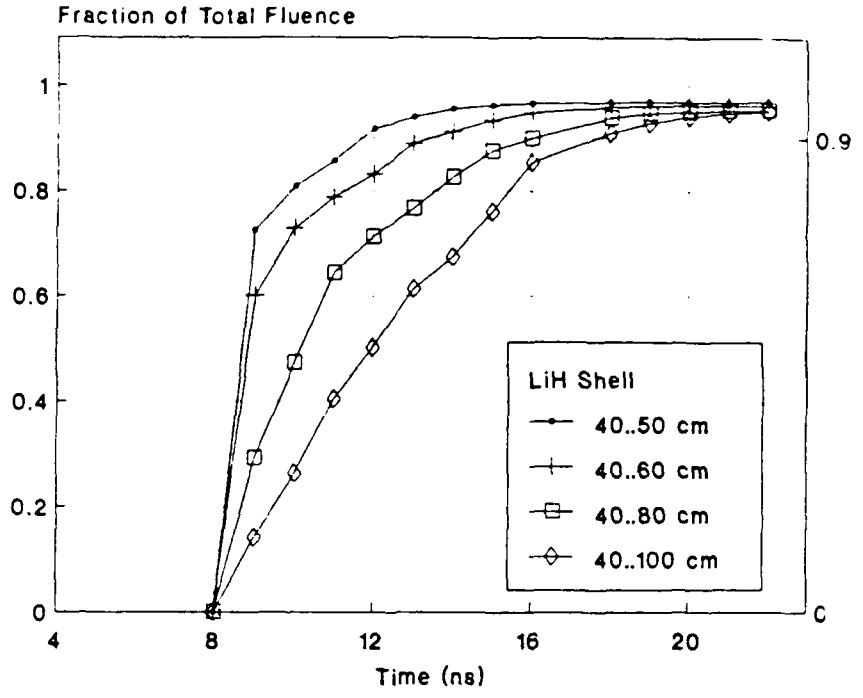

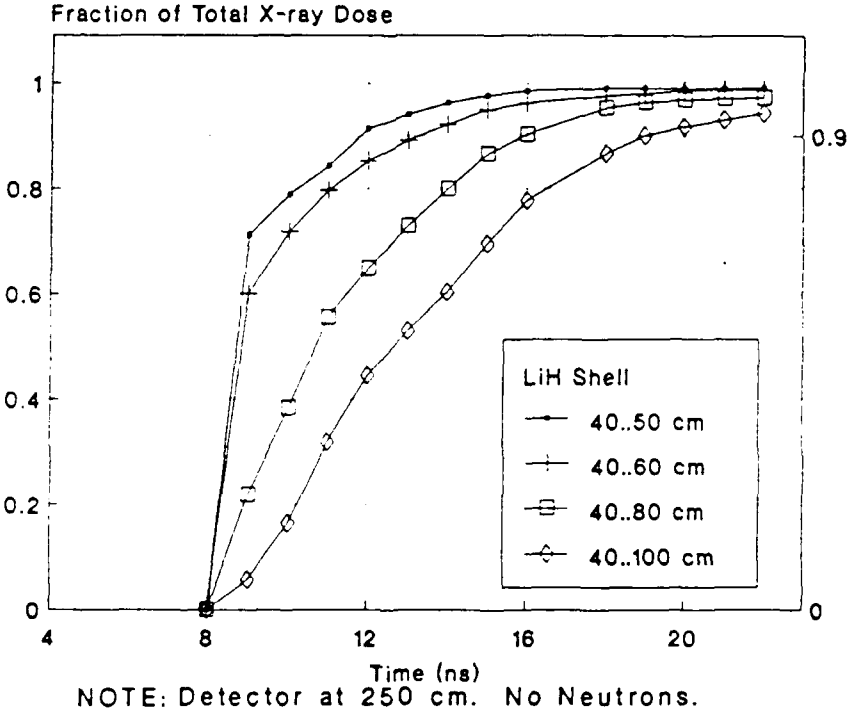

NOTE: Detector at 250 cm. No Neutrons.

Figure 3.1: Temporal Variations of X-ray Dose and Fluence with ^{7}LiH Thickness (Neutrons OFF)

The detector used in Figure 3.1 (and for most of the data presented in this thesis) was a point detector located 250 cm from the center of the chamber in free space. At 250 cm, spherical divergence of the source pulse would lead to less than a 15 percent variation in fluence over a 2 m surface located perpendicular to the axis of the chamber. The uniformity of the X-ray fluence is important to the fidelity of the simulation, in that a space vehicle would experience an almost planar X-ray pulse, and many effects can be geometry dependant.

Increasing the thickness of the LiH shell lengthened the arrival interval (T90) of the X-ray energy fluence from 3.5 ns at a 10 cm thickness to 10 ns at a 60 cm thickness. Similarly, the rise-time (T50) increased from less than 1 ns at 10 cm to 4 ns at 60 cm. In the process, the energy fluence was attenuated by 90 percent of the free field value.

The physics behind the relationship of the pulse length and rise-time to the thickness and outside diameter of the LiH shell can be explained as follows. When the initial pulse of X rays enters the inner wall of the LiH, many of them undergo multiple scatters before escaping through the outer wall of the LiH shell. The more an individual X ray scatters, the longer its path length and, therefore, the longer the time it takes to escape from LiH shell. As the

thickness of the shell is increased, the number of X rays that undergo multiple scatters increases as does the average number of scatters per photon; the collided pulse becomes longer (temporally) and takes on a longer rise-time, while the uncollided pulse is attenuated. Since the source pulse is instantaneous, the uncollided X-ray pulse has an instantaneous rise-time and no duration. As the ratio of collided X-ray fluence to uncollided X ray fluence increases, the pulse length and rise-time of the collided X rays increasingly dominate the temporal characteristics of the overall pulse. In the spherical geometry used in this work, there are two material thicknesses which affect the temporal qualities of the pulse: the thickness of the LiH shell and its outside diameter. The thickness of the shell determines the size of the uncollided portion of the pulse and, therefore, is the dominant characteristic governing the rise-time of the pulse. The diameter of the shell is the maximum thickness of LiH through which a singly-scattered X ray must pass, and is therefore strongly tied to the total pulse length.

One measure of the duration of a pulse of X rays is the Full Width at Half Maximum (FWHM) of the X-ray pulse. A plot of the normalized X-ray flux and dose rate (rads(Si)/sec) as a function of time outside a 60 cm LiH shell is presented in Figure 3.2. The standard deviation of each point is plotted beneath each of the dose and flux curves. The standard

deviation of each point is the difference between the standard deviation curve and the x axis. Both the dose rate and the flux have a FWHM of 7 to 8 ns for a 60 cm shell.

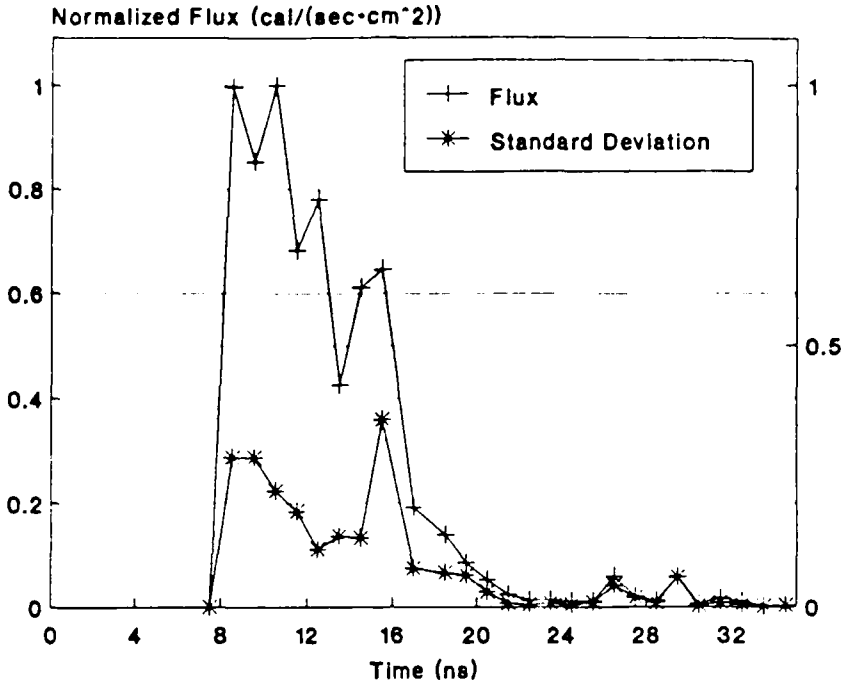

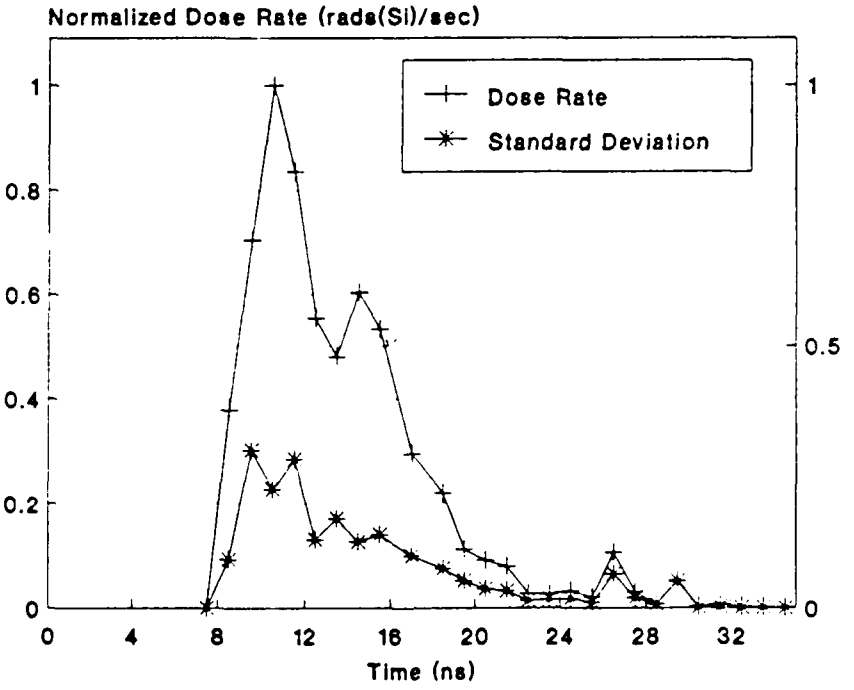

Note: Detector at 250 cm. 40..100 LIH Shell. No Neutrons.

Figure 3.2: X-ray Flux and Dose Rates Outside a ^{7}LiH Shell in an LMF Chamber

Spectral Shifts

To assess the effect of the scattering medium on the energy distribution of the X-ray spectrum, the resultant spectra from the calculations presented above were compared to the input X-ray spectrum. A plot comparing the input spectrum to the spectrum outside a 60 cm LiH shell is presented in Figure 3.3. LiH was chosen for the scattering medium because it had a very low absorption cross section for hard X rays. A hard X ray undergoing a collision in a LiH is usually scattered to a lower energy instead of being absorbed. On the other hand, the cross section for absorption of soft (low-energy) X rays is much higher than for hard X rays, so that a soft X ray undergoing a collision is almost always absorbed. When a pulse of X rays with a wide energy band enters the LiH shell, the high-energy X rays scatter down in energy and the low-energy X rays are absorbed. Thus, both ends of the spectrum diminish in magnitude, leaving a peak somewhere in the middle. The energy of this peak is determined by the characteristics of the scattering material, being higher for some than for others. In the LiH used for this work the peak energy shifted from the input spectrum peak of 37.5 keV to a final spectral peak of 25 keV. The final spectrum is more strongly peaked than the initial spectrum, an effect which

is more pronounced as the thickness of the LiH shell is increased.

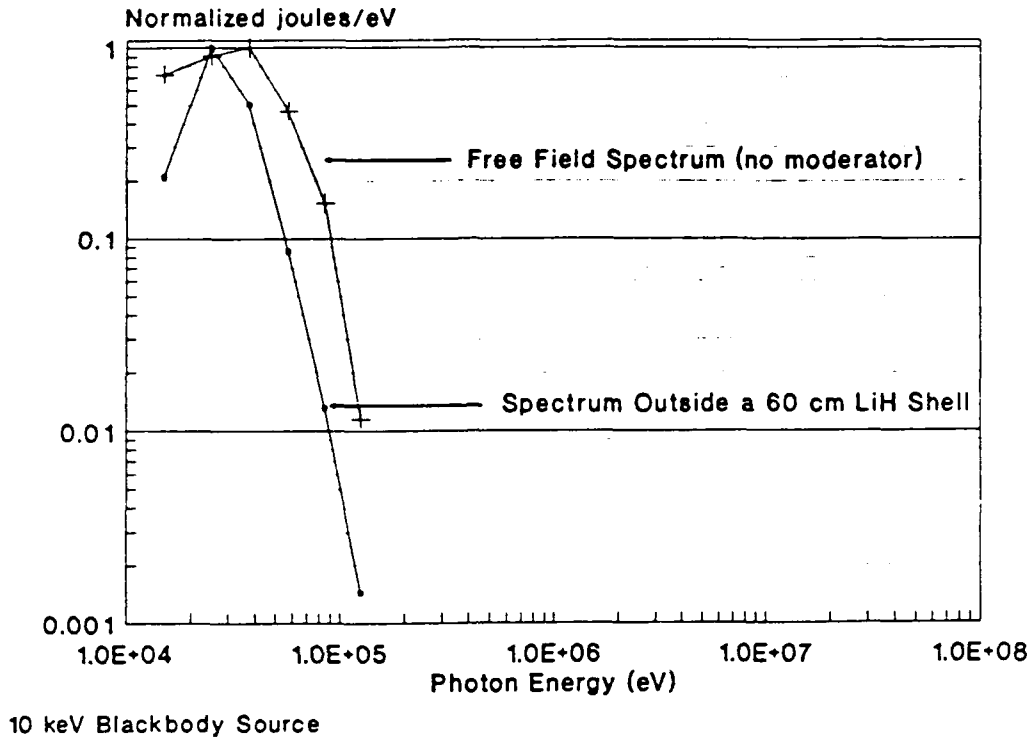

Figure 3.3: Peaking of the X-Ray Spectrum by ^{7}LiH

Neutron Effects

To assess the effects of the neutron component of the DT ICF pulse, a calculation was performed with the X rays turned 'off' and the neutrons turned 'on'. Neutrons interact with the materials in the chamber to produce neutron-capture gamma rays which could interfere with temporal and spectral fidelity of a hard X-ray simulation test. The neutrons themselves can be a problem if their energies and fluences

are sufficiently high. The gamma-ray spectrum and arrival times outside a 40 cm thick LiH shell in an LMF chamber are presented in Figure 3.4. The gamma-ray pulse consists of a strong peak around 2 MeV with a long, low-energy tail. The total gamma fluence at 250 cm was 36.6(+/- 1) cal/cm^2 and produced a dose of 480 (+/- 10) krad(Si). The gamma pulse began at 19 ns, but ninety-five percent of the pulse arrived after 100 ns. The total neutron fluence was $2(+/- 0.5)*10^{15}$ MeV-equivalent neutrons/cm^2. An examination of the secondary generation data produced by MORSE revealed that the majority of the energy of the neutron-generated gamma rays was formed by the capture of epithermal neutrons by the lithium hydride. The large number of scatters and the length of time necessary for the neutrons to slow down to energies where the capture cross section becomes appreciable made the process very time-consuming.

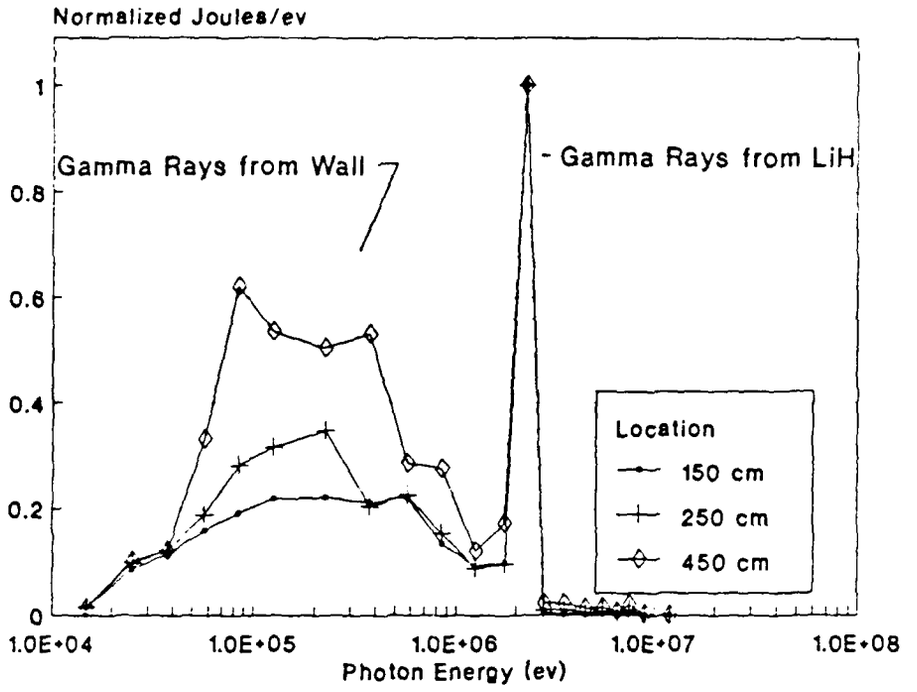

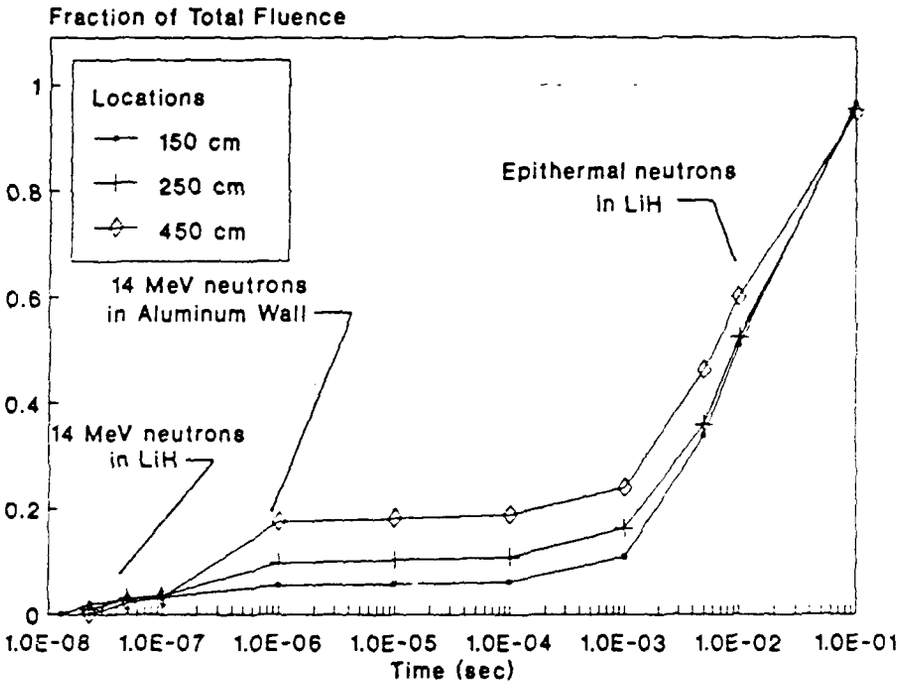

Note: 40..80 cm LiH Shell. Neutron Source Only

Figure 3.4: Neutron-generated Photons Outside a ^{7}LiH Shell in an LMF Chamber

Combined Calculations (Neutrons + X Rays)

To examine the combined effects of the source X rays and the neutron-generated gamma rays, separate calculations were performed with the LiH shell (40 cm thick) in free space and in the LMF chamber. A comparison of the temporal response at 250 cm is presented in Figure 3.5. Twenty percent of the total photon energy pulse was from gamma rays generated in the aluminum wall, 50% was from gamma rays generated in the LiH and only 30% was the original X-ray pulse. The temporal quality of the X-ray component, however, was not actually changed. Ninety percent of the total photon pulse which arrived by 100 ns arrived within the first of 10 ns of the total pulse; ninety-seven percent of the gamma-ray pulse arrived later than 100 ns.

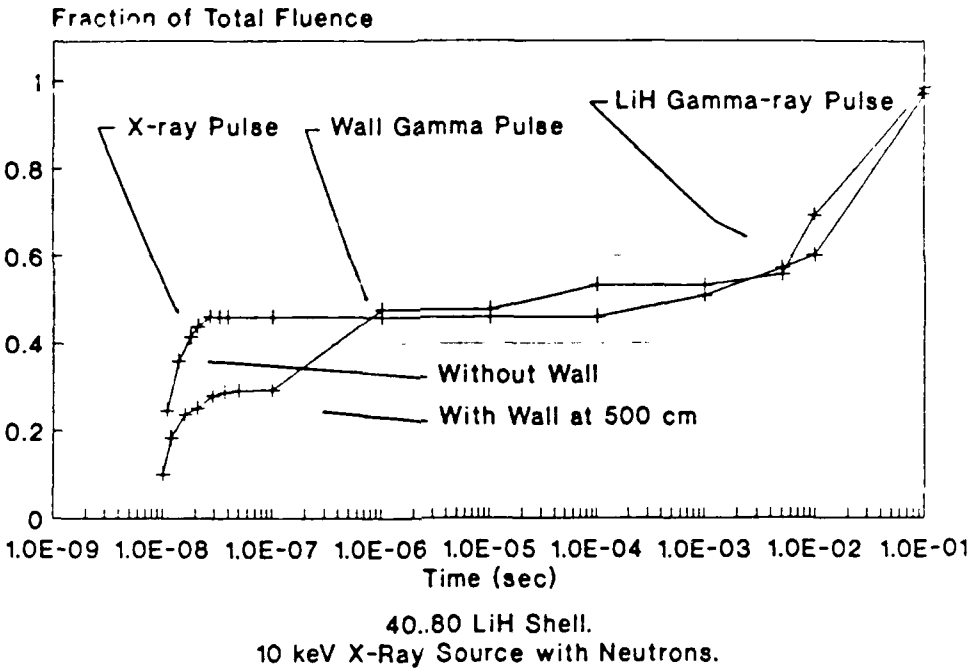

Figure 3.5: Arrival Times for X Rays and Gamma Rays Outside a ^{7}LiH Shell in an LMF Chamber with Neutrons ON

Response at a Graphite Cone

Since most of the energy of the gamma ray pulse is carried by high-energy photons, it might be argued that they are not significant due to their small interaction probability. Indeed, the unfiltered (surface) dose outside a 40 cm thick LiH shell was 15.6 Mrad(Si) from X rays compared to 0.48 Mrad(Si) from gamma rays. The filtered dose, however, is quite a different matter. After passing through the graphite surface of an RV and the aluminum casing of an electrical circuit, the high-energy component of the spectrum takes on a much greater significance due to the

attenuation of the lower-energy X rays. Figure 3.6 presents a comparison of the dose arrival time at a detector just outside the graphite RV shape in the LMF chamber to that of a detector located at the center of the aluminum/silicon shell inside the RV. Inside the graphite, the late-time photons comprise over 90 p[illegible]cent of the total fluence while comprising only 70 percent at the surface. About 30 percent of the surface dose (rads(carbon)) arrives after 100 ns, but still over 90 percent of the dose (rads(C)) at depth is generated by late-time gamma rays. Only a few percent of the silicon surface dose is late-time, but at depth the silicon dose still exhibits the strong stepped temporal characteristic with 70 percent of the total dose arriving after 100 ns.

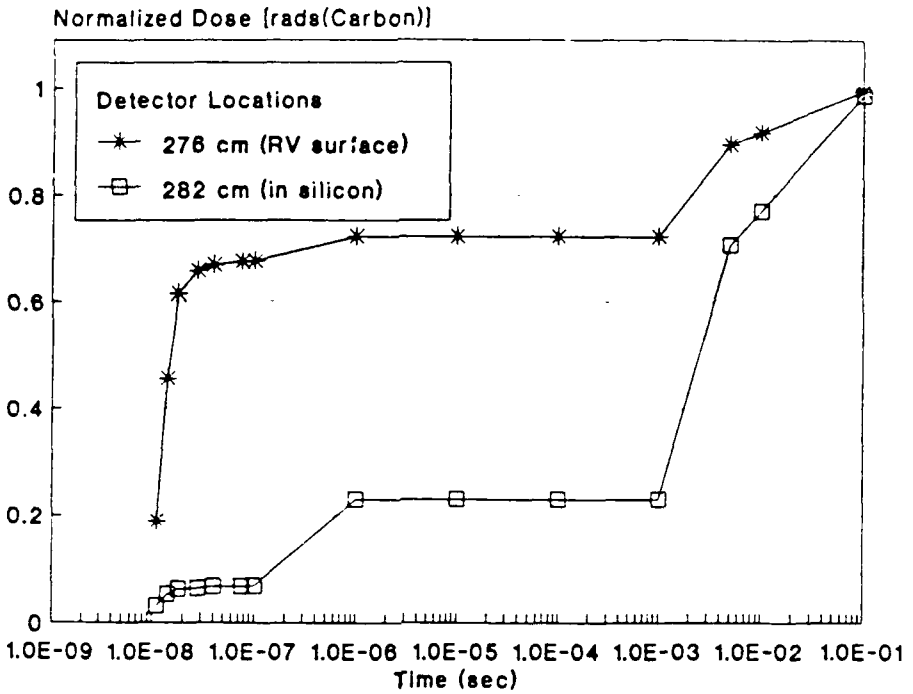

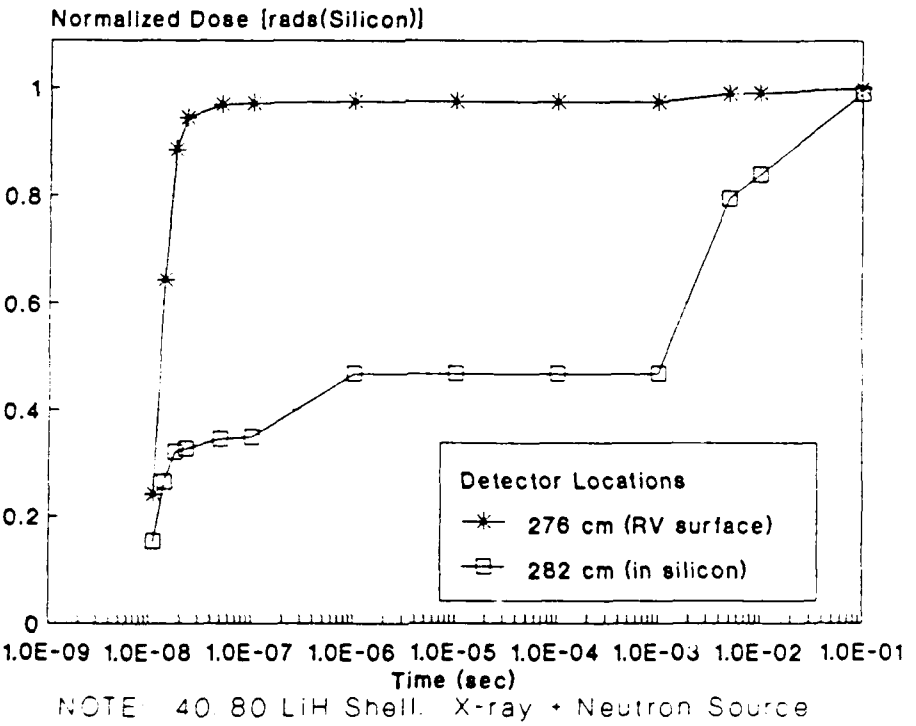

Figure 3.6: Dose in Carbon and Silicon from Photons Outside a ^{7}LiH Shell in an LMF Chamber

Reduction of Neutrons and Neutron-Capture Gamma Rays

A number of methods were examined to reduce the energy contribution from the gamma rays and to shorten the interval over which they were generated. Most of the gamma rays from the LiH were created by the capture of epithermal neutrons by the lithium. The isotope of lithium used was ^{7}Li, which captures high-energy (MeV range) neutrons and low-energy (epithermal) neutrons, but does not capture intermediate energy neutrons. The addition of ^{10}B (which has a high neutron capture cross section over a broad range of energies) at 10% normal atom density to the LiH reduced the time interval over which the gamma rays were generated in the scattering shell to less than 100 ns. These results are illustrated in Figure 3.7. At 250 cm, the gamma ray fluence was reduced to 7.1(+/-0.6) cal/cm^2 and the gamma ray dose to 160 (+/- 10) krads(Si). The neutron fluence was $9(+/-1)*10^{14}$ Mev-equivalent neutrons/cm^2. The 2 MeV gamma ray peak in the previous gamma-ray spectrum was eliminated but was replaced by a lower 0.478 MeV ^{10}B gamma-ray peak; the resulting photon spectrum had an endpoint energy of around 1 Mev. The addition of boron did not affect the gamma rays which were generated in the walls, nor did it significantly reduce the MeV-equivalent neutron fluence.

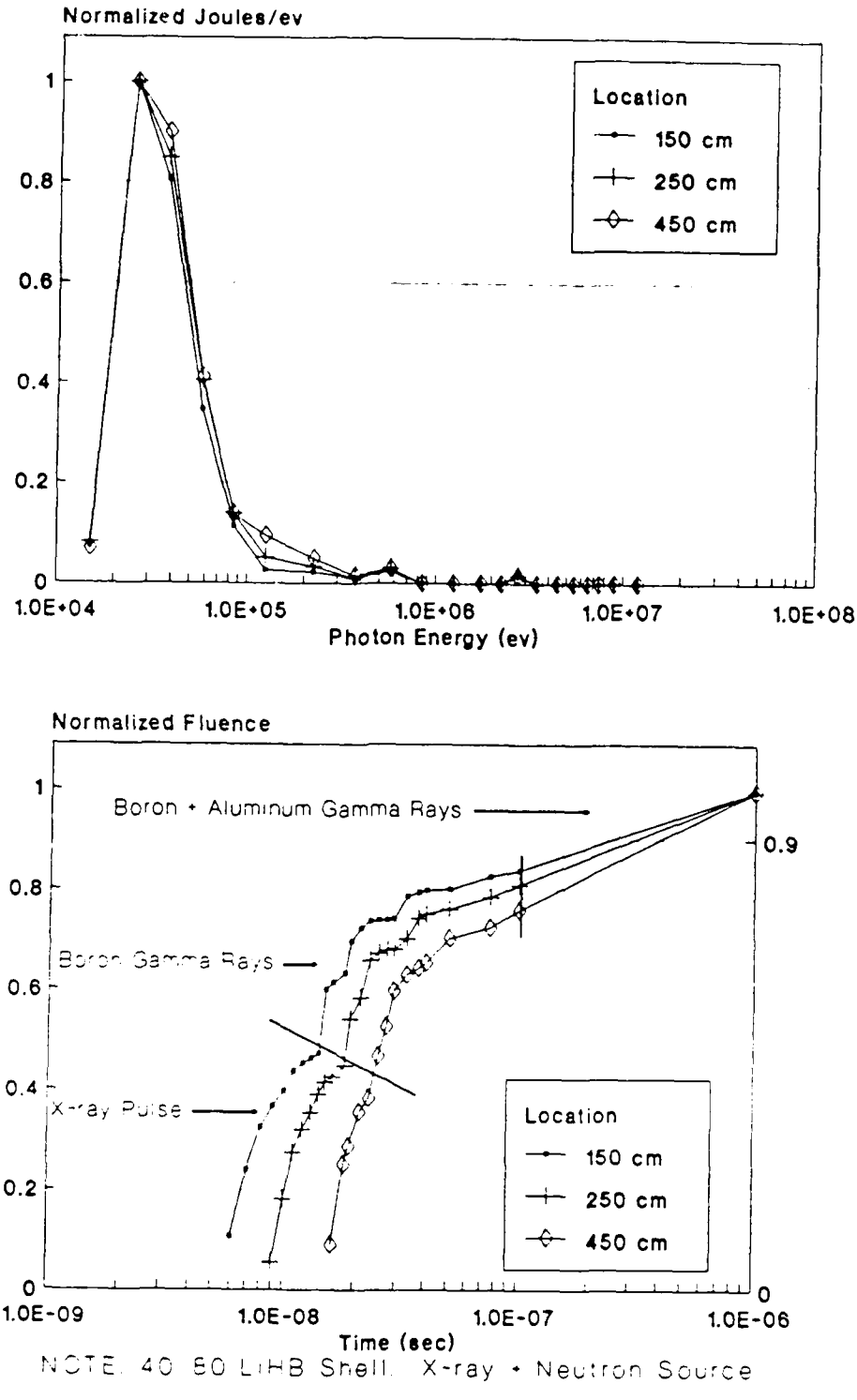

Figure 3.7: Detector Responses to Photons Outside a ^{7}LiHB Shell in an LMF Chamber

To reduce the fluence of neutrons scattered from the wall and the photon fluence from gamma rays generated in the wall, two shielding configurations -- one rectangular and one conical -- were used. Both shields consisted of a 1 m external blanket of LiH seeded with 10 percent boron to stop the neutrons, and a 5 cm internal lead liner to stop the neutron-capture gamma rays. Both shields began at 150 cm and extended to the wall, surrounding the detector locations and opening towards the borated LiH shell. Runs were made with the 40..80 (inner radius..outer radius), 60..80, and 20..40 cm scattering shells of borated lithium hydride. The temporal and spectral photon responses for both shields were comparable; the photon response for the 40..80 shell is presented in Figure 3.8. At locations deep inside the shield, the photon energy fluence after 100 ns (which includes the wall gamma rays plus late gamma rays from the boron) was reduced from 30% to 10% of the total photon energy fluence. The responses from the thinner shells were roughly equivalent to each other. However, they differed from that of the 40..80 shell in that their temporal response rose rapidly to a plateau at 60 percent of the total response by about 20 ns, then rose gradually in several steps and slopes to better than 98 percent of the total response at one microsecond. The total pulse lengths were still longer than desired and the MeV-equivalent-

neutron fluence was not significantly affected by the presence of the shields.

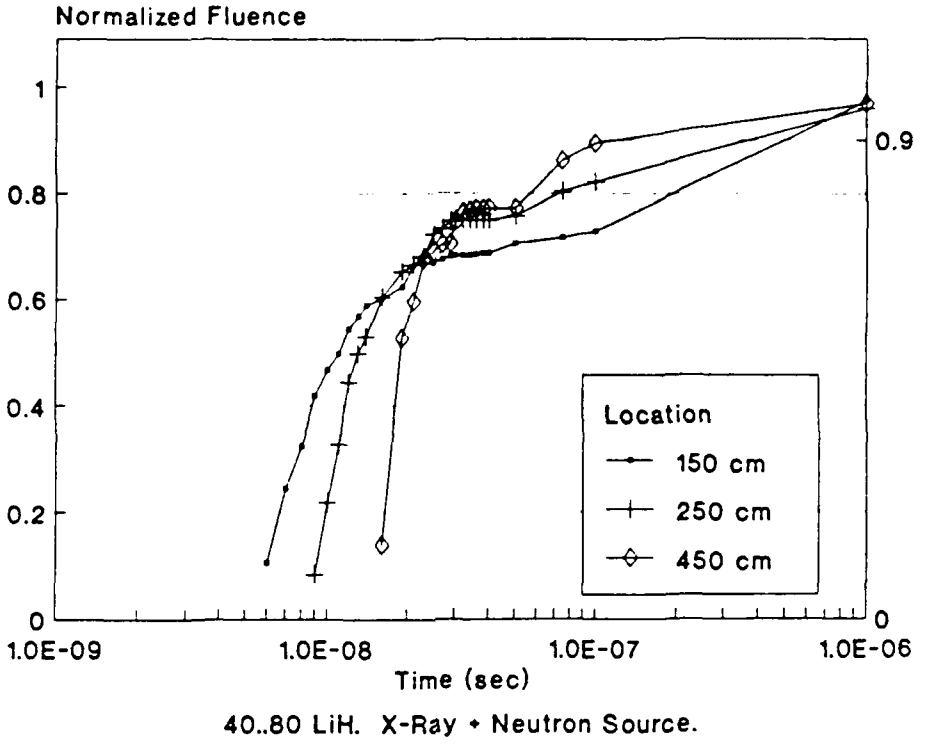

Figure 3.8: Shielded Photon Fluence Outside a ^{7}LiHB Shell in an LMF Chamber

Since the neutron-^{7}Li reaction was the major contributor of gamma rays, a number of calculations were made using pure ^{6}LiH as the scattering medium. These calculations were made with the RV turned "off" and with a cylindrical shield about the detector locations. The shield extended from 150 cm to the wall, had an inner radius of 100 cm, and had a 20 cm thick outer layer natural tungsten and a 20 cm thick inner layer of LiH. The previous chamber wall (1 m thick aluminum) was replaced with a more realistic wall composed of an 8 cm aluminum inner wall, a 1 m thick blanket of

borated water (0.01% ^{10}B), and an 8 cm aluminum outer wall. The fluences and doses from these calculations are presented in Table 3.2; the photon spectrum is presented in Figure 3.9 and the arrival times for various thicknesses of LiH scattering shells are presented graphically in Figure 3.10. In these calculations the diameter of the LiH shell was held constant and the inner radius varied. As a result, the 90% arrival times were roughly equivalent for all thicknesses of LiH but the rise-time increased with the shell thickness.

Table 3.2: Variation in Photon Fluence, Dose and Arrival Interval with ^{6}LiH Thickness

Inner radius (cm)	LiH Shell (cm)	Photon Fluence (cal/cm^2)	Photon Dose (MRads(Si))	Neutron* Fluence ($10^{14}/cm^2$)
80	00	80(1)	72(2)	
70	10	51(3)	47(2)	300(100)
60	20	36(2)	32(2)	50(18)
50	30	25(1)	23(2)	30(9)
40	40	18(1)	18(1)	6(2)
30	50	14(2)	13(1)	3(0.9)
10	60	10.8(1)	9.3(.7)	0.8(0.2)

*Read as 10^{14}Mev-equivalent neutrons/cm^2.

Note: Detector was located at 250 cm in free space. Neutrons were turned 'on' in these runs. Numbers in brackets are the standard deviations of the values they follow.

The minimum neutron fluence in these runs was 8 (+/- 2)*10^{13} neutrons/ cm^2, much closer to the desired levels, and the contribution of neutron capture gamma rays was negligible. The photon spectrum was essentially identical to the X-ray spectrum, with no evidence of a high-energy tail. At a

thickness of 60 cm there remained sufficient fluences of photons to be of interest to VLE work. Further, the use of a more realistic chamber wall seems to have eliminated the large neutron-capture gamma-ray contribution from the aluminum.

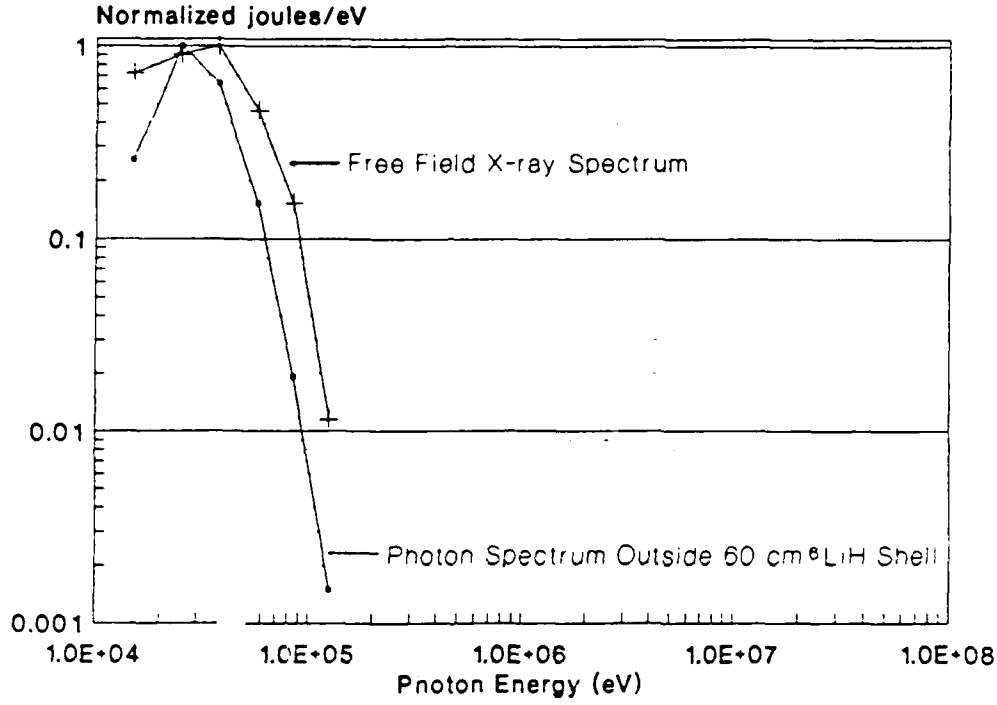

Figure 3.9: Photon Spectrum (X + Gamma Rays) Outside a 60 cm ^{6}LiH Shell (Neutrons ON)

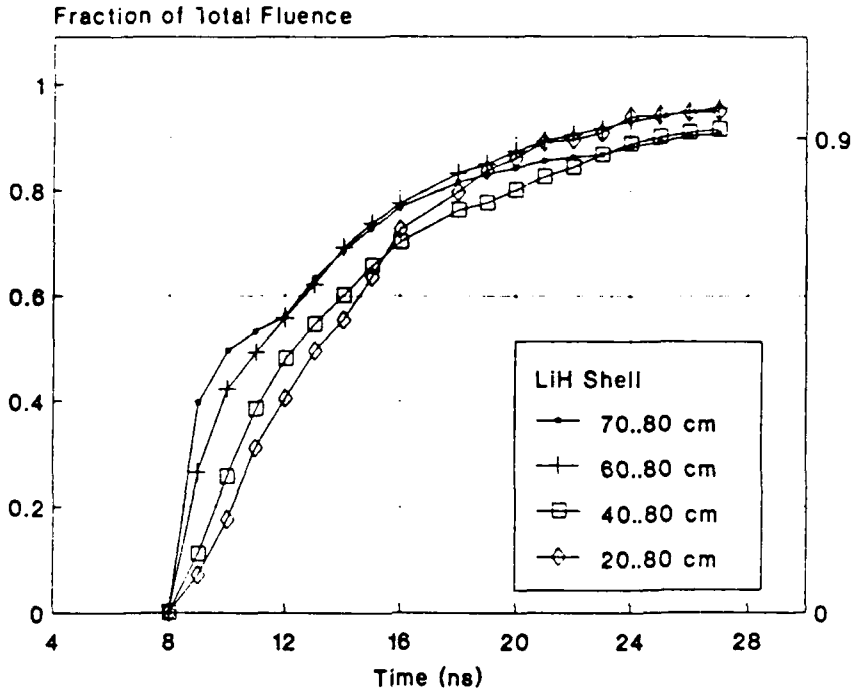

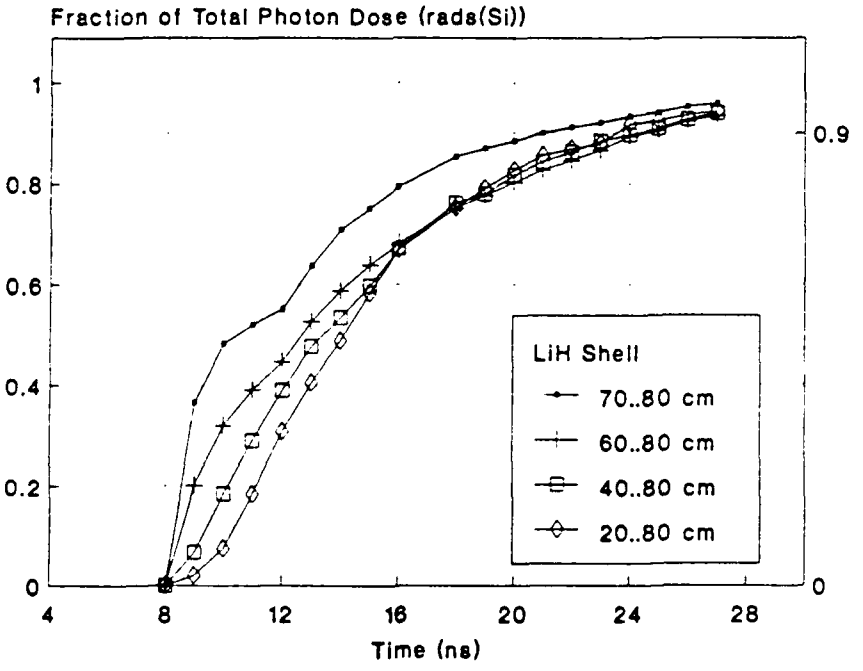

10 keV X-Ray Source with Neutrons.

Figure 3.10: Temporal Variations of X-ray Dose and Fluence with ^{6}LiH Thickness (Neutrons ON)

A broad variety of shadow shields were used in an attempt to reduce the neutron fluences while retaining sufficient X-ray intensity to be of interest to VLE work. Without a shadow shield, the smallest one-MeV-equivalent neutron fluence calculated in this work was $8*10^{13}$ neutrons/cm^2. Although the results were not conclusive, calculations using a tungsten shadow shield inside the LiH shell indicate that it may be possible to reduce the neutron fluence by 50% while reducing the X-ray intensity by the same percentage. Reduction below 50% through the use of shadow shields alone seems unlikely, however, since the presence of the shield seems to increase the scattered contribution from the region of the LiH shell not shadowed by the shield.

IV. Summary and Recommendations

Summary

Using a scattering medium of ^{6}LiH, it is possible to temporally stretch the initial X-ray pulse so that 90 percent of the X-ray energy incident on the detector arrives over a period of 15 ns. In doing so, 87 percent of the initial X-ray energy (with photon energy greater than 10 keV) is absorbed in the LiH, and the spectrum of the X-ray pulse is significantly softened. The remaining X-ray pulse retains sufficient intensity and spectral quality to be of interest to the VLE community. The total X-ray dose outside a 60 cm shell of ^{6}LiH was 9.3 Mrads(Si) with 50 percent arriving over an interval of 6 ns. This corresponds to a dose rate $8*10^{14}$ rads(Si)/sec. Messenger and Ash(2:412,413) cite hardness levels for a number of devices that are in the range of doses found in these calculations; the dose rates encountered in this work, however, exceeded the highest dose rates given in any of the charts presented in their text (10^{12} rads(Si)/sec) indicating that additional temporal stretching and dose attenuation may be necessary(2:421-428).

The large fraction of neutrons produced by the DT reaction, however, pose a significant engineering problem to the use of the LMF as an X-ray weapons effects simulator. Neutrons scatter off the LiH, losing energy until they reach an energy level at which the neutron capture cross section is appreciable. When the neutrons are captured, some of the capturing nuclei emit high-energy gamma rays, which themselves scatter and contribute to the total photon fluence on the target. For a LiH shell containing only ^{7}Li, this process takes an extended period of time, when compared to the time scale of initial pulse, and could be a real problem if the diagnostics cannot discriminate against the late-time photons generated. Adding ^{10}B to the LiH to absorb the neutrons before they interact with the ^{7}Li does not completely solve the problem, but substitution of the isotope ^{6}Li for ^{7}Li reduces the intensity of the pulse of gamma rays generated in the LiH to levels which are insignificant when compared to the X-ray intensity. This is not a particularly attractive solution, however, due to the high cost of ^{6}Li. Further work needs to be done to determine the isotopic composition of Li which would maintain a sufficiently low level of ^{7}Li neutron-capture gamma rays.

Elimination of significant intensities of neutron-capture gamma rays does not eliminate the problems the neutrons pose to hard X-ray weapons effects simulation. The fluence of the neutrons themselves is high enough to present severe problems to tests involving semiconductor devices. In the calculations performed for this work, about 87 percent of the total source energy was in the form of neutrons. The minimum neutron fluence obtained in this work was on the order of 10^{14} n/cm^2. According to Messenger and Ash(2:200,401), neutron effects on semiconductors begin at around 10^{12} n/cm^2 with many devices hardened to the 10^{13} n/cm^2 range. Calculations using shadow shields, though inconclusive at this point, indicate that it may be possible to reduce the neutron fluence by 50% and still retain sufficient X-ray intensity. If a suitable shielding configuration is discovered the neutron fluences may not be a problem. If real-time diagnostics are used in the simulations, it may be possible to diagnostically separate the neutron effects from the X-ray effects. 14 MeV neutrons travel much slower than photons; the neutrons arrive at a point 325 cm from the source 60 ns after the photons. If the diagnostics can take advantage of this interval, meaningful X-ray information could be gained even if the neutrons interfered with the effects being studied.

Recommendations for Further Work

This work examined a large number of chamber configurations using LiH as a scattering medium, and attempted to minimize the fluence of gamma-rays generated by the neutrons from the DT reaction. This effort included adding shields and reflectors, many of which are not discussed here, but all of which had severely limited usefulness. ^{10}B was added to the LiH to eliminate the problem of gamma rays generated in the LiH, and while this did reduce the gamma intensity and pulse length, it was not as effective as could be hoped. The substitution of 100% ^{6}Li for the lithium in the LiH was found to reduce the gamma ray intensity to sufficiently low levels for VLE work. Further work is needed to determine the exact isotopic composition of the lithium required to keep the gamma ray levels sufficiently low. Other scattering media, such as carbon and beryllium, as well as other neutron absorbers such as cadmium, hafnium and indium should also be investigated. Boron was an interesting absorber choice because its use did not introduce an activation problem. Other choices will need to be carefully evaluated in this regard.

The use of shadow shields offers great promise in further reducing the fluence of energetic neutrons. The most promising shield was a conical shield composed of a layer of tungsten (to slow down the fast neutrons) followed by a

dense borated hydrogenous medium (to further slow and absorb the neutrons), followed by another tungsten layer (to stop the gamma rays).

Conclusion

While the neutrons produced in the DT reaction pose significant problems to the use of the LMF to simulate the effects of hard X rays from nuclear weapons, there is evidence that these problems are not insurmountable. Although further work in this area is needed, adequate shielding should be able to reduce the neutron fluence to acceptable levels while stretching the temporal response of the X-ray pulse to a length, intensity and spectral quality to be of interest to the VLE community.

Appendix A

User-written Routines

Overview

The MORSE computer program is supplied as a series of Fortran subroutines that perform the functions common to all problems the program is designed to handle. The user supplies the problem-specific subroutines, and compiles and links all the subroutines together to form the executable program. This appendix presents a brief discussion of the function of each subroutine used in this work, followed by the source code for all the subroutines. The subroutines were written in Fortran 77 and were compiled and run on a VAX under the VMS operating system.

Description of the Subroutines

Main. This is the main controlling module of the program. It allocates all of the common memory blocks, reads in the input and output file names, and terminates the program.

Bankr. Bankr is, as its name implies, the banker of the MORSE system. Just like an actual banker, it is consulted any time a significant event occurs in the life of a particle, such as a birth, collision or boundary crossing. It is Bankr that calls the flux estimator routines Relcol, Sdata and Sgam.

Direc. Direc is a required user-written function. It must be in the code, but doesn't really do anything in this application.

Gtmed. The purpose of this function is to assign a different media to a particular zone other than that assigned in the data file. In this application, the routine simply sets the media for each zone to that assigned in the data file.

Relcol, Sdata and Sgam. Relcol is a routine used to estimate the flux at a point detector. At each collision, Bankr calls Relcol which determines (through subroutine calls) the probability per unit steradian of a particle

being emitted in the direction of the detector, the number of mean free paths to the detector, and the distance to the detector.

The contribution of the particle to the total fluence at the detector is then calculated as (5:4.6-39):

$$Con=Wate*Pro(mu,E)*exp(-mfp)/Dist^2, \qquad (1)$$

where:

Con	is the contribution of the particle to the fluence at the detector,
Wate	is the weight of the particle leaving the collision site,
Pro(mu,E)	is the probability per unit steradian that the particle scatters to outgoing energy group *E with direction cosine mu*,
exp()	is the exponential operator,
mfp	is the number of mean free paths between the collision site and the detector, and
$Dist^2$	is the square of the distance to the detector.

This contribution is then multiplied by the average energy of the particle energy bin (taken as the simple average of the upper and lower energy of the bin) to produce an energy fluence in ev/cm^2, and passed to the bookkeeping routines along with the age of the particle.

It should be noted, however, that Eq.(1) is only good for contributing events that occur at distances greater than one centimeter from a detector. Nearer than this the formula begins to blow up, approaching infinity as the distance approaches zero. For this reason, detectors should always be located one centimeter from the nearest surface on which a source event or collision could occur; the code contains a provision to skip this calculation and print a warning should the distance to the detector be less than one centimeter.

Sdata and Sgam perform the same function as Relcol (and are actually modifications of Relcol), but at different points in the particle lifetime. Sdata sends information to the bookkeeping routines when the particle is generated at the beginning of the batch. These data form the uncollided portion of the total fluence, and the probability per steradian of a particle having direction cosine mu is taken as 1/(4 pi). Sgam sends information at the birth of a secondary particle, and is identical to Sdata except that the fluence information is stored as collided fluence.

There are a number of TYPE statements included in these routines. These are to print diagnostic information in case the program encounters a geometry problem.

Source. Source is the subroutine that generates the source particles. It determines the energy group of the source particles from the input energy spectrum and determines their direction cosines randomly from a discrete, isotropic angular distribution. Source also sets the initial weight of each particle to the weight specified by the user in the data input file.

Fortran Source Code

```
C * * THIS IS THE MAIN ROUTINE * * * * * * * * * * * * * * * * * * * * * * *
C * * Based on a routine by D. Beller Aug 88.  3 blanket regions,          *
C * * 4 detectors                                                          *
C * * Modified by Don Nichols Sept 88 for RV in LMF chamber                *
C
C**************************************************************************
C*        This version determines uncollided fluence using estimators     *
C*         to calculate the contribution of each source and collision     *
C*          event to the flux at a point detector.                        *
C**************************************************************************
C
C * * THE FOLLOWING CARD DETERMINES THE SIZE ALLOWED FOR BLANK COMMON
C * * The value of NLFT below should be set to one less than this size
C
      COMMON NC(600001)
C
C * * NOTE - THE ORDER OF COMMONS IN THIS ROUTINE IS IMPORTANT AND MUST
C * * CORRESPOND TO THE ORDER USED IN DUMP ROUTINES SUCH AS HELP, XSCHLP
C * *
C * * LABELLED COMMONS FOR WALK ROUTINES    * * * * * * * * * * * * * * * *
      COMMON /APOLLO/ AGSTRT,DDF,DEADWT(26),ITOUT,ITIN
      COMMON /FISBNK/ MFISTP
      COMMON /NUTRON/ NAME
C * *
C * * LABELLED COMMONS FOR CROSS-SECTION ROUTINES  * * * * * * * * * * * *
      COMMON /LOCSIG/ ISCCOG
      COMMON /MEANS/ NM
      COMMON /MOMENT/ NMOM
      COMMON /QAL/ Q
      COMMON /RESULT/ POINT
C * *
C * * LABELLED COMMONS FOR GEOMETRY INTERFACE ROUTINES  * * * * * * * * *
      COMMON /GEOMC/ XTWO
      COMMON /NORMAL/ UNORM
C * *
C * * LABELLED COMMONS FOR USER ROUTINES  * * * * * * * * * * * * * * * * *
      COMMON /PDET/ ND
      COMMON /USER/ AGST
C * *
C * * COMMON /DUMMY/ WILL NOT BE FOUND ELSEWHERE IN THE PROGRAM  * * * * *
      COMMON /DUMMY/ DUM
C * *
        CHARACTER*40, NAM1
        CHARACTER*40, NAM2
        TYPE *,' '
        TYPE *,'********* MORSE Code, LMF-ICF Problem *********'
        TYPE *,'========> WARNING !!! <========'
        TYPE *,'ABORT if mixed x-secs are not assigned to FOR010'
        TYPE *,' '
        TYPE *,'ENTER NAME OF INPUT FILE'
        ACCEPT 100, NAM1
100     FORMAT(A40)
        TYPE *,'ENTER NAME OF OUTPUT FILE'
        ACCEPT 200, NAM2
200     FORMAT (A40)
        OPEN(UNIT=1,NAME=NAM1,TYPE='OLD')
        OPEN(UNIT=2,NAME=NAM2,TYPE='NEW')
      ITOUT = 2
      ITIN = 1
        NLFT=600000
      CALL MORSE(NLFT)
        TYPE 300, NAM2
300     FORMAT(X,'OUTPUT FILE IS ',A40)
      STOP
      END
```

```
      SUBROUTINE BANKR(NBNKID)
C  DO NOT CALL EUCLID FROM BANKR(7)
      COMMON /APOLLO/ AGSTRT,DDF,DEADWT(5),ETA,ETATH,ETAUSD,UINP,VINP,
     1 WINP,WTSTRT,XSTRT,YSTRT,ZSTRT,TCUT,XTRA(10),
     2   I0,I1,MEDIA,IADJM,ISBIAS,ISOUR,ITERS,ITIME,ITSTR,LOCWTS,LOCFWL,
     3 LOCEPR,LOCNSC,LOCFSN,MAXGP,MAXTIM,MEDALB,MGPREG,MXREG,NALB,
     4 NDEAD(5),NEWNM,NGEOM,NGPQT1,NGPQT2,NGPQT3,NGPQTG,NGPQTN,NITS,
     5 NKCALC,NKILL,NLAST,NMEM,NMGP,NMOST,NMTG,NOLEAK,NORMF,NPAST,
     6 NPSCL(13),NQUIT,NSIGL,NSOUR,NSPLT,NSTRT,NXTRA(10)
      COMMON /NUTRON/ NAME,NAMEX,IG,IGO,NMED,MEDOLD,NREG,U,V,W,UOLD,VOLD
     1 ,WOLD,X,Y,Z,XOLD,YOLD,ZOLD,WATE,OLDWT,WTBC,BLZNT,BLZON,AGE,OLDAGE
      NBNK = NBNKID
      IF (NBNK) 100,100,140
  100 NBNK = NBNK + 5
      GO TO (104,103,102,101),NBNK
  101 CALL STRUN
C     CALL HELP(4HSTRU,1,1,1,1)
      RETURN
  102 NBAT = NITS - ITERS
      NSAVE = NMEM
      CALL STBTCH(NBAT)
C   NBAT IS THE BATCH NO. LESS ONE
c   This lets us know where we are in the run
      TYPE 3333, NBAT+1
 3333 FORMAT (1X,'Running batch Number',2X,I4)
      RETURN
  103 CALL NBATCH(NSAVE)
C   NSAVE IS THE NO. OF PARTICLES STARTED IN THE LAST BATCH
      RETURN
  104 CALL NRUN(NITS,NQUIT)
C   NITS IS THE NO. OF BATCHES COMPLETED IN THE RUN JUST COMPLETED
C   NQUIT .GT. 1 IF MORE RUNS REMAIN
C         .EQ. 1 IF THE LAST SCHEDULED RUN HAS BEEN COMPLETED
C         IS THE NEGATIVE OF THE NO. OF COMPLETE RUNS, WHEN AN
C               EXECUTION TIME KILL OCCURS
      RETURN
  140 GO TO (1,2,3,4,5,6,7,8,9,10,11,12,13),NBNK
C  NBNKID   COLL TYPE   BANKR CALL      NBNKID   COLL TYPE   BANKR CALL
C     1      SOURCE     YES (MSOUR)       2      SPLIT      NO  (TESTW)
C     3      FISSION    YES (FPROB)       4      GAMGEN     YES (GSTORE
C     5      REAL COLL  YES (MORSE)       6      ALBEDO     YES (MORSE)
C     7      BDRYX      YES (NXTCOL)      8      ESCAPE     YES (NXTCOL
C     9      E-CUT      NO  (MORSE)      10      TIME KILL  NO  (MORSE)
C    11      R R KILL   NO  (TESTW)      12      R R SURV   NO  (TESTW)
C    13      GAMLOST    NO  (GSTORE)
    1 CALL SDATA
      RETURN
    2 RETURN
    3 RETURN
    4 CALL SGAM
      TYPE *,'another gamma in batch ',nbat+1
      RETURN
    5 CALL RELCOL
      numcol=numcol+1
      if (numcol.GT.500) then
          numcol=0
          TYPE *,'another 500 collisions in batch ',nbat+1
      endif
      RETURN
    6 RETURN
    7 continue
c     TYPE *,'another boundary crossing in batch ',nbat+1
      RETURN
    8 RETURN
    9 RETURN
   10 RETURN
   11 TYPE *,'another one bites the dust in batch ',nbat+1
      RETURN
   12 RETURN
```

```
13 RETURN
   END
```

```
      FUNCTION DIREC(F)
      direc=1.
      return
      end
C * *
C * *
C * * Subroutine GTMED gets the media for each zone
C     this version each zone has it's own cross section assigned
      SUBROUTINE GTMED(MDGEOM,MDXSEC)
      MDXSEC=MDGEOM
      RETURN
      END
```

```
      SUBROUTINE RELCOL
C
C   THIS VERSION IS FOR POINT DETECTORS LOCATED AT (XD,YD,ZD)
C
      COMMON /USER/ AGSTRT,WTSTRT,XSTRT,YSTRT,ZSTRT,DFF,EBOTN,EBOTG,
     1 TCUT,I0,I1,IADJM,NGPQT1,NGPQT2,NGPQT3,NGPQTG,NGPQTN,NITS,NLAST,
     2 NLEFT,NMGP,NMTG,NSTRT
      COMMON /PDET/ ND,NNE,NE,NT,NA,NRESP,NEX,NEXND,NEND,NDNR,NTNR,NTNE,
     1 NANE,NTNDNR,NTNEND,NANEND,LOCRSP,LOCXD,LOCIB,LOCCO,LOCT,LOCUD,
     2 LOCSD,LOCQE,LOCQT,LOCQTE,LOCQAE,LMAX,EFIRST,EGTOP
      COMMON /NUTRON/ NAME,NAMEX,IG,IGO,NMED,MEDOLD,NREG,U,V,W,UOLD,VOLD
     1 ,WOLD,X,Y,Z,XOLD,YOLD,ZOLD,WATE,OLDWT,WTBC,BLZNT,BLZON,AGE,OLDAGE
      COMMON BL(1)
      DIMENSION NL(1)
      EQUIVALENCE (BL(1),NL(1))
      DATA NEST /1/, FNEST /1./
C   NEST + FNEST ARE THE NO. OF ESTIMATES TO BE MADE TO EACH DETECTOR
C * * * ISTAT MUST BE EQUAL TO 1.
C * * * NEX MUST BE AT LEAST 1
C * * * NEXND MUST BE AT LEAST 1
C     ********************************************************************
C     THIS ROUTINE REDUCES THE NUMBER OF THERMAL NEUTRONS TRACKED
C             THRU THE GEOMETRY BY 90% AND THEN COMPENSATES BY
C             MULTIPLYING THE WEIGHT OF THE REMAINING 10% BY 10.
C     ********************************************************************
      CHECK=1.
      IF (IGO.NE.28) GO TO 100
      XI= FLTRNF(0)
      IF (XI.GE.0.1) RETURN
      CHECK=10.
100   CONTINUE
      DO 30 I=1,ND
      IA=LOCXD+I
      XE = BL(IA)
      YE = BL(IA+ND)
      ZE = BL(IA+2*ND)
      A = XE - X
      B = YE - Y
      C = ZE - Z
      SD2=A*A+B*B+C*C
      DS=SQRT (SD2)
C * * * COS DEPENDS ON THE ANGLE OF INTEREST
      COS=C/DS
      THETA = (A*UOLD + B*VOLD + C*WOLD)/DS
      IGOLD = IGO
      IGO = NGPQT3
      IF (IGO.LE.NGPQT1) IGO=NGPQT1
      IA = LOCRSP + NRESP*NMTG + 1
      CALL PTHETA(NMED,IGOLD,IGO,THETA,BL(IA),NMTG)
      NES = 0
      PSUM = 0.
      IA = IA - 1
      DO 5 IL=IGOLD,IGO
 5    PSUM = PSUM + ABS (BL(IA+IL))
 10   R = FLTRNF(0) * PSUM
      DO 15 IL=IGOLD,IGO
      IF (R-ABS (BL(IA+IL))) 20,20,15
 15   R = R - ABS (BL(IA+IL))
      IL = IGO
 20   MARK=1
      AGED = AGE + DS/BL(NMTG+IL)
      MEDIUM=NMED
      CALL EUCLID(MARK,X,Y,Z,XE,YE,ZE,DS,IL,ARG,0,MEDIUM,BLZNT,NREG)
      if (ARG.NE.-160) GO TO 21
      TYPE *,'g1  IT HAPENED AGAIN'
      TYPE 300,I
 300  FORMAT(X,'DETECTOR ',6X,I4)
      TYPE 301, NMED
 301  FORMAT(X,'-MEDIUM ',6X,I4)
```

```
      TYPE 302, MEDOLD
  302 FORMAT(X,'-OLDMEDIUM ',6X,I4)
      TYPE 303, NREG
  303 FORMAT(X,'-REGION ',6X,I4)
      TYPE 304, IBLZN
  304 FORMAT(X,'-ZONE ',6X,I4)
      TYPE 305,IBLZO
  305 FORMAT(X,'-OLDZONE ',6X,I4)
      TYPE *, 'RELCOL'
   21 IF (ARG.LT.-64.) GO TO 25
C********BEWARE THIS VERSION WILL NOT WORK IF ENERGY BIASING IS USED
      IF (SD2.LT.1.0) then
          TYPE *, 'Threw out a particle...WARNING.....'
          GO TO 25
      endif
      CON = CHECK*WATE*EXP (ARG)*SIGN (PSUM,BL(IA+IL))/SD2/FNEST
      IF (CON.LT.1.E-38) GO TO 25
      IF ((IL.NE.NGPQT2).AND.(IL.NE.NMTG)) THEN
         AVENG=(BL(IL)+BL(IL+1))/2.0
      ELSEIF (IL.EQ.NGPQT2) THEN
      AVENG=(BL(IL)+EBOTN)/2.0
      ELSE
      AVENG=(BL(IL)+EBOTG)/2.0
      ENDIF
      CON=CON*AVENG
      CALL FLUXST (I,IL,CON,AGED,COS,0)
   25 NES = NES + 1
      INN=LOCXD+6*ND+I
      NL(INN)=NL(INN)+1
      IF (NES-NEST) 10,30,30
   30 CONTINUE
      RETURN
      END
```

```
      SUBROUTINE SDATA
C
C     THIS VERSION IS FOR POINT DETECTORS LOCATED AT (XD,YD,ZD)
C
      COMMON /USER/ AGSTRT,WTSTRT,XSTRT,YSTRT,ZSTRT,DFF,EBOTN,EBOTG,
     1 TCUT,IO,I1,IADJM,NGPQT1,NGPQT2,NGPQT3,NGPQTG,NGPQTN,NITS,NLAST,
     2 NLEFT,NMGP,NMTG,NSTRT
      COMMON /PDET/ ND,NNE,NE,NT,NA,NRESP,NEX,NEXND,NEND,NDNR,NTNR,NTNE,
     1 NANE,NTNDNR,NTNEND,NANEND,LOCRSP,LOCXD,LOCIB,LOCCO,LOCT,LOCUD,
     2 LOCSD,LOCQE,LOCQT,LOCQTE,LOCQAE,LMAX,EFIRST,EGTOP
      COMMON /NUTRON/ NAME,NAMEX,IG,IGO,NMED,MEDOLD,NREG,U,V,W,UOLD,VOLD
     1 ,WOLD,X,Y,Z,XOLD,YOLD,ZOLD,WATE,OLDWT,WTBC,BLZNT,BLZON,AGE,OLDAGE
      COMMON EN(1)
C       ********************************************************************
      FNEST=1.0
      DO 25 I=1,ND
      IA=LOCXD+I
      XE = EN(IA)
      YE = EN(IA+ND)
      ZE = EN(IA+2*ND)
      A = XE - X
      B = YE - Y
      C = ZE - Z
      SD2=A*A+B*B+C*C
      DS=SQRT (SD2)
C * * * COS DEPENDS ON THE ANGLE OF INTEREST
      COS=C/DS
      AGED=DS/EN(NMTG+IG)+AGE
 20   MARK=1
      MEDIUM=NMED
      CALL EUCLID(MARK,X,Y,Z,XE,YE,ZE,DS,IG,ARG,0,MEDIUM,BLZNT,NREG)
      if (ARG.NE.-160) GO TO 21
      TYPE *,'g1  IT HAPENED AGAIN'
      TYPE 300,I
 300  FORMAT(X,'DETECTOR ',6X,I4)
      TYPE 301, NMED
 301  FORMAT(X,'-MEDIUM ',6X,I4)
      TYPE 302, MEDOLD
 302  FORMAT(X,'-OLDMEDIUM ',6X,I4)
      TYPE 303, NREG
 303  FORMAT(X,'-REGION ',6X,I4)
      TYPE 304, IBLZN
 304  FORMAT(X,'-ZONE ',6X,I4)
      TYPE 305,IBLZO
 305  FORMAT(X,'-OLDZONE ',6X,I4)
      TYPE *, 'SDATA'
 21   IF (ARG.LT.-64.) GO TO 25
C********BEWARE THIS VERSION WILL NOT WORK IGNORES COLLISIONS CLOSE TO
C********            DETECTOR
      IF (SD2.LT.1.0)  THEN
          TYPE *, 'Threw out a particle...WARNING.....'
          GO TO 25
      ENDIF
      CON = WATE*EXP (ARG)/12.56637/SD2/FNEST
      IF (CON.LT.1.E-38) GO TO 25
      IF ((IG.NE.NGPQT2).AND.(IG.NE.NMTG)) THEN
         AVENG=(EN(IG)+EN(IG+1))/2.0
      ELSEIF (IG.EQ.NGPQT2) THEN
      AVENG=(EN(IG)+EBOTN)/2.0
      ELSE
      AVENG=(EN(IG)+EBOTG)/2.0
      ENDIF
      CON=CON*AVENG
C  *   *  SWITCH=1  -- STORE IN ALL RELEVANT ARRAYS
      CALL FLUXST (I,IG,CON,AGED,COS,1)
 25   CONTINUE
      RETURN
      END
```

```
      SUBROUTINE SGAM
C
C     THIS VERSION IS FOR POINT DETECTORS LOCATED AT (XD,YD,ZD)
C
      COMMON /USER/ AGSTRT,WTSTRT,XSTRT,YSTRT,ZSTRT,DFF,EBOTN,EBOTG,
     1 TCUT,IO,I1,IADJM,NGPQT1,NGPQT2,NGPQT3,NGPQTG,NGPQTN,NITS,NLAST,
     2 NLEFT,NMGP,NMTG,NSTRT
      COMMON /PDET/ ND,NNE,NE,NT,NA,NRESP,NEX,NEXND,NEND,NDNR,NTNR,NTNE,
     1 NANE,NTNDNR,NTNEND,NANEND,LOCRSP,LOCXD,LOCIB,LOCCO,LOCT,LOCUD,
     2 LOCSD,LOCQE,LOCQT,LOCQTE,LOCQAE,LMAX,EFIRST,EGTOP
      COMMON /NUTRON/ NAME,NAMEX,IG,IGO,NMED,MEDOLD,NREG,U,V,W,UOLD,VOLD
     1 ,WOLD,X,Y,Z,XOLD,YOLD,ZOLD,WATE,OLDWT,WTBC,BLZNT,BLZON,AGE,OLDAGE
      COMMON EN(1)
C     ****************************************************************
      FNEST=1.0
      DO 25 I=1,ND
      IA=LOCXD+I
      XE = EN(IA)
      YE = EN(IA+ND)
      ZE = EN(IA+2*ND)
      A = XE - X
      B = YE - Y
      C = ZE - Z
      SD2=A*A+B*B+C*C
      DS=SQRT (SD2)
C * * * COS DEPENDS ON THE ANGLE OF INTEREST
      COS=C/DS
      AGED=DS/EN(NMTG+IG)+AGE
 20   MARK=1
      MEDIUM=NMED
      CALL EUCLID(MARK,X,Y,Z,XE,YE,ZE,DS,IG,ARG,0,MEDIUM,BLZNT,NREG)
       if (ARG.NE.-160) GO TO 21
      TYPE *,'gf  IT HAPENED AGAIN'
      TYPE 300,I
 300  FORMAT(X,'DETECTOR ',6X,I4)
      TYPE 301, NMED
 301  FORMAT(X,'-MEDIUM ',6X,I4)
      TYPE 302, MEDOLD
 302  FORMAT(X,'-OLDMEDIUM ',6X,I4)
      TYPE 303, NREG
 303  FORMAT(X,'-REGION ',6X,I4)
      TYPE 304, IBLZN
 304  FORMAT(X,'-ZONE ',6X,I4)
      TYPE 305,IBLZO
 305  FORMAT(X,'-OLDZONE ',6X,I4)
      TYPE *, 'SGAM'
  21  IF (ARG.LT.-64.) GO TO 25
C********BEWARE THIS VERSION WILL NOT WORK IF COLLISION IS CLOSE TO
C********            DETECTOR
      IF (SD2.LT.1.0) THEN
           TYPE *, 'Threw out a particle...WARNING.....'
           GO TO 25
      ENDIF
      CON = WATE*EXP (ARG)/12.56637/SD2/FNEST
      IF (CON.LT.1.E-38) GO TO 25
      IF ((IG.NE.NGPQT2).AND.(IG.NE.NMTG)) THEN
         AVENG=(EN(IG)+EN(IG+1))/2.0
      ELSEIF (IG.EQ.NGPQT2) THEN
      AVENG=(EN(IG)+EBOTN)/2.0
      ELSE
      AVENG=(EN(IG)+EBOTG)/2.0
      ENDIF
      CON=CON*AVENG
C  *  *  SWITCH=0  -- STORE IN ALL RELEVANT ARRAYS EXCEPT UD
      CALL FLUXST (I,IG,CON,AGED,COS,0)
 25   CONTINUE
      RETURN
      END
```

```
      SUBROUTINE SOURCE(IG,U,V,W,X,Y,Z,WATE,MED,AG,ISOUR,ITSTR,NGPQT3,
     1   DDF,ISBIAS,NMTG)
      COMMON /USER/ DUM(9),I0,I1,IDUM(12)
      COMMON WTS(1)
C
C   IF ITSTR=0, MUST PROVIDE IG,X,Y,Z,U,V,W,WATE AND AG IF DESIRED TO BE
C     DIFFERENT FROM CARD VALUES (WHICH ARE THE VALUES INPUT TO SOURCE)
C   IF ITSTR=1, IG IS THE GRP NO. CAUSING FISSION, MUST PROVIDE NEW IG
C     THIS VERSION OF  SOURCE  SELECTS INITIAL GROUP FROM THE INPUT SPEC
C
      DATA ICALL/1/
      IF (ICALL) 10,10,5
 5    ICALL = 0
      WRITE (I0,1000)
 1000 FORMAT (' YOU ARE USING THE DEFAULT VERSION OF SOURCE WHICH SETS W
     1ATE TO DDF AND PROVIDES AN ENERGY IG.')
 10   IF(ISOUR)15,15,60
 15   WATE=DDF
      IF (ISBIAS) 20,20,25
 20   NWT = 2*NMTG
      GO TO 30
 25   NWT = 3*NMTG
 30   R = FLTRNF(0)
      DO 35 I=1,NGPQT3
      IF (R - WTS(I+NWT)) 40,40,35
 35   CONTINUE
 40   IG=I
      IF (ISBIAS) 60,60,45
 45   IF (I-1) 60,50,55
 50   WATE = WATE*WTS(2*NMTG+1)/WTS(3*NMTG+1)
      GO TO 60
 55   WATE = WATE*(WTS(2*NMTG+I)-WTS(2*NMTG+I-1))/(WTS(3*NMTG+I)-WTS(3*N
     1MTG+I-1))
C     ******************************************************************
C     This version of the MORSE SOURCE file is modified for a
C     problem with the point source directed ISOTROPICALLY.
C     ******************************************************************
 60   Z     = 0.0
      Y     = 0.0
      X     = 0.0
 99   CALL GTISO(U,V,W)
      RETURN
      END
```

Appendix B

Example of MORSE Data Input File

Data is entered into the MORSE program at run time in the form of a data input file, with the format of each record precisely determined by the format statements in the source code and documented in the manuals that accompany MORSE (5:ch 4). This appendix presents a sample data input file, that was used to calculate the temporal and spectral photon fluence at positions inside a shielded cavity in an LMF chamber, outside a LiHF shell.

```
Problem to determine neutron/xray fluence on rv in lmf chamber
  100  250   20    :   37   21   37   58    0    0  200    6    0
    0   58    0    01.0        1.000E-5   1.0E4     0         4.384E3
       0.0         0.0         0.0         0.0         0.0         0.0         0.0
 0.000E+00 0.000E+00 0.000E+00 2.075E-04 4.574E-05 2.640E-05 4.627E-05
 4.326E-05 3.474E-05 2.921E-05 2.454E-05 2.947E-05 3.500E-05 5.498E-06
 1.383E-05 2.435E-05 1.926E-05 3.095E-06 2.276E-05 4.931E-05 4.853E-05
 2.922E-05 1.571E-06 1.358E-06 3.207E-07 1.848E-08 5.756E-08 1.646E-08
 1.635E-09 1.837E-10 6.859E-11 1.701E-12 1.382E-13 1.915E-09 5.820E-09
 5.655E-09 3.008E-09 0.000E+00 0.000E+00 0.000E+00 0.000E+00 0.000E+00
 0.000E+00 0.000E+00 0.000E+00 0.000E+00 0.000E+00 0.000E+00 3.705E-28
 8.732E-18 7.781E-12 5.299E-06 1.430E-04 9.741E-04 4.475E-03 7.510E-03
 8.213E-03 9.415E-03
 1.9600 +7 1.6900 +7 1.4900 +7 1.4200 +7 1.3800 +7 1.2800 +7 1.2200 +7
 1.1100 +7 1.0000 +7 9.0500 +6 8.1900 +6 7.4100 +6 6.3800 +6 4.9700 +6
 4.7200 +6 4.0700 +6 3.0100 +6 2.3900 +6 2.3100 +6 1.8300 +6 1.1100 +6
 5.5000 +5 1.5800 +5 1.1100 +5 5.2500 +4 2.4800 +4 2.1900 +4 1.0300 +4
 3.3500 +3 1.2300 +3 5.8300 +2 1.0100 +2 2.9000 +1 1.0700 +1 3.0600 +0
 1.1300 +0 4.1400 -1 1.4000 +7 1.0000 +7 8.0000 +6 7.0000 +6 6.0000 +6
 5.0000 +6 4.0000 +6 3.0000 +6 2.5000 +6 2.0000 +6 1.5000 +6 1.0000 +6
 7.0000 +5 4.5000 +5 3.0000 +5 1.5000 +5 1.0000 +5 7.0000 +4 4.5000 +4
 3.0000 +4 2.0000 +4
A00045FA231A
    0    1    0    0    0   14   58
    1    1   58    0    0    0   0.00 +0    0.05 +0    0.30 -0    0.00 +0
   -1
    0    0    0    0
 6.8968 -1 7.0830 -1 8.2761 -1 8.6715 -1 9.0565 -1 9.3775 -1 9.5540 -1
 9.7981 -1 9.3460 -1 8.6250 -1 7.7562 -1 6.7991 -1 5.1535 -1 4.1567 -1
 3.8802 -1 2.9512 -1 1.4341 -1 1.1907 -1 1.0094 -1 7.0092 -2 1.6321 -3
 4.1979 -4 9.3777 -4 6.9061 -4 2.1888 -3 9.5333 -3 5.8675 -3 1.4911 -2
 4.3375 -3 2.9440 -3 4.5123 -3 7.7552 -3 1.4483 -2 2.3680 -2 4.3302 -2
 6.6392 -2 2.5024 -1
 6.8968 -1 7.0830 -1 8.2761 -1 8.6715 -1 9.0565 -1 9.3775 -1 9.5540 -1
 9.7981 -1 9.3460 -1 8.6250 -1 7.7562 -1 6.7991 -1 5.1535 -1 4.1567 -1
 3.8802 -1 2.9512 -1 1.4341 -1 1.1907 -1 1.0094 -1 7.0092 -2 1.6321 -3
 4.1979 -4 9.3777 -4 6.9061 -4 2.1888 -3 9.5333 -3 5.8675 -3 1.4911 -2
 4.3375 -3 2.9440 -3 4.5123 -3 7.7552 -3 1.4483 -2 2.3680 -2 4.3302 -2
 6.6392 -2 2.5024 -1
 6.8968 -1 7.0830 -1 8.2761 -1 8.6715 -1 9.0565 -1 9.3775 -1 9.5540 -1
 9.7981 -1 9.3460 -1 8.6250 -1 7.7562 -1 6.7991 -1 5.1535 -1 4.1567 -1
 3.8802 -1 2.9512 -1 1.4341 -1 1.1907 -1 1.0094 -1 7.0092 -2 1.6321 -3
 4.1979 -4 9.3777 -4 6.9061 -4 2.1888 -3 9.5333 -3 5.8675 -3 1.4911 -2
 4.3375 -3 2.9440 -3 4.5123 -3 7.7552 -3 1.4483 -2 2.3680 -2 4.3302 -2
 6.6392 -2 2.5024 -1
 4.2579-02 4.4749-0  4.5484-02 4.5334-02 4.6163-02 4.8756-02 5.3471-02
 6.1778-02 6.8680-02 7.4906-02 7.9445-02 8.2633-02 8.4593-02 8.0525-02
 7.6957-02 6.5722-02 4.8608-02 4.6932-02 4.7877-02 3.8039-02 2.1191-02
 2.2625-02 3.2514-02 3.6203-02 4.4126-02 4.9916-02 5.9324-02 9.5856-02
 1.4010-01 1.9895-01 3.4229-01 4.9102-01 6.6312-01 7.2693-01 8.5372-01
 8.5359-01 9.0211-01
 1.1534 -1 1.1556 -1 1.4724 -1 1.7432 -1 1.9183 -1 2.2580 -1 2.5199 -1
 2.9974 -1 2.5090 -1 2.3222 -1 1.9442 -1 2.1901 -1 1.2837 -1 9.4951 -3
 0.0000 +0 0.0000 +0 0.0000 +0 0.0000 +0 0.0000 +0 0.0000 +0 0.0000 +0
 0.0000 +0 0.0000 +0 0.0000 +0 0.0000 +0 0.0000 +0 0.0000 +0 8.4146 -8
 3.0231 -6 5.2711 -6 1.0771 -5 3.2221 -5 4.8580 -5 6.5050 -5 1.2286 -4
 2.4098 -4 7.8900 -4
 1.2076 -1 1.7137 -1 1.9054 -1 1.9112 -1 1.8096 -1 1.6907 -1 1.9144 -1
 1.5227 -1 1.2607 -1 1.2114 -1 9.2448 -2 3.3317 -2 2.9578 -5 1.5745 -5
 1.3695 -5 1.0544 -5 1.1807 -5 1.2513 -5 9.2964 -6 7.0412 -6 5.2936 -6
 4.8693 -6 6.5696 -6 8.4378 -6 1.2044 -5 1.4972 -5 1.9074 -5 3.1704 -5
 5.3990 -5 8.1745 -5 1.5665 -4 3.2645 -4 5.6955 -4 1.0051 -3 1.7526 -3
 2.8862 -3 5.6442 -3
 1.2076 -1 1.7137 -1 1.9054 -1 1.9112 -1 1.8096 -1 1.6907 -1 1.9144 -1
 1.5227 -1 1.2607 -1 1.2114 -1 9.2448 -2 3.3317 -2 2.9578 -5 1.5745 -5
 1.3695 -5 1.0544 -5 1.1807 -5 1.2513 -5 9.2964 -6 7.0412 -6 5.2936 -6
 4.8693 -6 6.5696 -6 8.4378 -6 1.2044 -5 1.4972 -5 1.9074 -5 3.1704 -5
 5.3990 -5 8.1745 -5 1.5665 -4 3.2645 -4 5.6955 -4 1.0051 -3 1.7526 -3
 2.8862 -3 5.6442 -3
```

```
0.0000 +0 0.0000 +0 0.0000 +0 0.0000 +0 0.0000 +0 0.0000 +0 0.0000 +0
0.0000 +0 0.0000 +0 0.0000 +0 0.0000 +0 0.0000 +0 0.0000 +0 0.0000 +0
0.0000 +0 0.0000 +0 0.0000 +0 0.0000 +0 0.0000 +0 0.0000 +0 0.0000 +0
0.0000 +0 0.0000 +0 0.0000 +0 0.0000 +0 0.0000 +0 0.0000 +0 0.0000 +0
0.0000 +0 0.0000 +0 0.0000 +0 0.0000 +0 0.0000 +0 0.0000 +0 0.0000 +0
0.0000 +0 0.0000 +0
0.0000 +0 0.0000 +0 0.0000 +0 0.0000 +0 0.0000 +0 0.0000 +0 0.0000 +0
0.0000 +0 0.0000 +0 0.0000 +0 0.0000 +0 0.0000 +0 0.0000 +0 0.0000 +0
0.0000 +0 0.0000 +0 0.0000 +0 0.0000 +0 0.0000 +0 0.0000 +0 0.0000 +0
0.0000 +0 0.0000 +0 0.0000 +0 0.0000 +0 0.0000 +0 0.0000 +0 0.0000 +0
0.0000 +0 0.0000 +0 0.0000 +0 0.0000 +0 0.0000 +0 0.0000 +0 0.0000 +0
0.0000 +0 0.0000 +0
0.0000 +0 0.0000 +0 0.0000 +0 0.0000 +0 0.0000 +0 0.0000 +0 0.0000 +0
0.0000 +0 0.0000 +0 0.0000 +0 0.0000 +0 0.0000 +0 0.0000 +0 0.0000 +0
0.0000 +0 0.0000 +0 0.0000 +0 0.0000 +0 0.0000 +0 0.0000 +0 0.0000 +0
0.0000 +0 0.0000 +0 0.0000 +0 0.0000 +0 0.0000 +0 0.0000 +0 0.0000 +0
0.0000 +0 0.0000 +0 0.0000 +0 0.0000 +0 0.0000 +0 0.0000 +0 0.0000 +0
0.0000 +0 0.0000 +0
6.8968 -1 7.0830 -1 8.2761 -1 8.6715 -1 9.0565 -1 9.3775 -1 9.5540 -1
9.7981 -1 9.3460 -1 8.6250 -1 7.7562 -1 6.7991 -1 5.1535 -1 4.1567 -1
3.8802 -1 2.9512 -1 1.4341 -1 1.1907 -1 1.0094 -1 7.0092 -2 1.6321 -3
4.1979 -4 9.3777 -4 6.9061 -4 2.1888 -3 9.5333 -3 5.8675 -3 1.4911 -2
4.3375 -3 2.9440 -3 4.5123 -3 7.7552 -3 1.4483 -2 2.3680 -2 4.3302 -2
6.6392 -2 2.5024 -1
6.8635 -1 8.8263 -1 1.0700 +0 1.1290 +0 1.1491 +0 1.1235 +0 1.0736 +0
1.0100 +0 8.9200 -1 7.4553 -1 6.3844 -1 5.6448 -1 4.1341 -1 2.5573 -1
2.7199 -1 2.6387 -1 1.6838 -1 1.3687 -1 6.8722 -2 3.1076 -3 3.4212 -4
2.5433 -4 2.1924 -3 1.8890 -3 1.1506 -2 5.0166 -3 4.1328 -4 3.5530 -4
5.9051 -4 9.0755 -4 1.7346 -3 3.6174 -3 6.3156 -3 1.1070 -2 1.9275 -2
3.1626 -2 1.2561 -1
8.3850-01 7.3784-01 1.1264+00 1.2668+00 1.2237+00 1.1661+00 1.0970+00
1.0302+00 1.0439+00 1.1636+00 1.2727+00 1.2537+00 9.4621-01 7.9580-01
6.6431-01 3.4698-01 1.6637-01 1.2875-01 1.2630-01 7.9409-02 1.8774-02
8.5742-04 9.2761-04 5.6459-04 9.1579-04 3.7896-04 1.0528-03 1.0625-03
1.0713-03 1.1696-04 1.9896-04 5.4378-04 8.1424-04 1.5741-03 2.5007-03
3.1035-03 1.2747-02
0.0000 +0 0.0000 +0 0.0000 +0 0.0000 +0 0.0000 +0 0.0000 +0 0.0000 +0
0.0000 +0 0.0000 +0 0.0000 +0 0.0000 +0 0.0000 +0 0.0000 +0 0.0000 +0
0.0000 +0 0.0000 +0 0.0000 +0 0.0000 +0 0.0000 +0 0.0000 +0 0.0000 +0
0.0000 +0 0.0000 +0 0.0000 +0 0.0000 +0 0.0000 +0 0.0000 +0 0.0000 +0
0.0000 +0 0.0000 +0 0.0000 +0 0.0000 +0 0.0000 +0 0.0000 +0 0.0000 +0
0.0000 +0 0.0000 +0
  0     0         COMBINATORIAL GEOMETRY OF LMF CHAMBER WITH RV
 SPH      0.         0.        0.       20.0
 SPH      0.         0.        0.       40.0
 SPH      0.         0.        0.       41.0
 TRC      0.         0.       -35.       0.        0.        30.
          1.        0.5
 RCC      0.         0.       -500.      0.        0.        465.
          5.
 RCC      0.         0.       -500.      0.        0.        460.
          6.
 SPH      0.         0.        0.      499.0
 SPH      0.         0.        0.      500.0
 SPH      0.         0.        0.      600.0
 TRC     302.804   0.0      -96.875   -24.804   0.       198.43
         25.0      0.
 RCC     288.      0.       50.       262.      0.       0.
         5.
 RCC     318.      0.       -75.      232.      0.       0.
         5.
 TRC     302.804   0.       -97.87    -25.5     0.       204.
         26.       0.
 RCC     288.      0.        50.      262.      0.       0.
         6.
 RCC     308.      0         -75.     232.      0.       0.
         6.
 SPH      0.         0.        0.      1000.0
 SPH      0.         0.        0.      1600.0
```

```
 SPH      0.          0.          0.          70.0
 TRC      0.          0.          0.          278.0      0.          0.
          0.          100.
 SPH      282.        0.          0.          2.4
 SPH      282.        0.          0.          2.6540
 SPH      282.        0.          0.          1.1
 BOX      150.0       -135.0      -215.       450.       0.          0.
          0.          270.0       0.          0.         0.          430.0
 BOX      250.0       -35.00      -115.       350.       0.          0.
          0.          70.00       0.          0.         0.          230.0
 BOX      150.0       -30.00      -110.       450.       0.          0.
          0.          60.00       0.          0.         0.          220.0
 END
 STM  10      +4
 PED  10 OR   +5OR  +11OR  +12
 WAL  10      +9     -8     -5     -11    -12
 LiH  10 OR   +2     -1     -4     -5OR   +23     +7     -24    -25
 RV   10      +10    -11    -12    -21
 ICE  10      +3     -2     -5     -4
 ICE  10 OR   +6     +7     -5     -3OR   +13     -10    -14    -15OR  +15
              +7     -12    -10OR  +8     -7     -12    -11    -5OR   +14
              +7     -11    -10
 VOD  10 OR   +1     -4     -5OR   22
 VOD  10 OR   +7     -13    -14    -15    -6     -3     -5     -4     -23
         OR   +25    +7     +23    -14    -15    -13
 EXT  10      +16    -9
 Asi  10      +21    -20
 sil  10      +20    -22
 LED  10      +24    +7     -25
 EXT  10      +17    -16
 END
   1    2    3    4    5    6    7    8    9   10   11   12   13   14
   1    1    1    2 1000 1000 1000 1000 1000 1000 1000 1000    6    0
37 GROUP N  CROSS SECTIONS --- P3 --- 21 GROUP GAMMA CROSS SECTIONS
  37   37   21   21   58   61    4    6    6    6    4    2    1    3
   0    0    0    0    0    0    0  -10    0    0    0
SAMBO ANALYSIS INPUT DATA  LMF-RV Problem
   6   34   55  -47    0    6    1    1
    150.9        0.0        0.0
    250.0        0.0        0.0
    275.9        0.0        0.0
    282.0        0.0        0.0
    350.9        0.0        0.0
    450.0        0.0        0.0
RESULTS of LMF-RV MORSE calculation
(1 Mev equivalent neutrons/cm^2/source particle    )
3.208 -06 3.429 -06 3.543 -06 3.553 -06 3.490 -06 3.396 -06 3.254 -06
3.059 -06 2.828 -06 2.831 -06 3.070 -06 2.093 -06 1.155 -06 1.156 -06
9.899 -07 9.161 -07 1.136 -06 1.082 -06 1.403 -06 1.362 -06 1.838 -06
2.728 -06 4.078 -07 1.051 -06 0.000 -05 0.000 -05 0.000 -05 0.000 -04
0.000 -04 0.000 -03 0.000 -03 0.000  02 0.000 -02 0.000 -01 0.000 -01
0.000      0.000      0.         0.         0.         0.         0.
0.         0.         0.         0.         0.         0.         0.
0.         0.         0.         0.         0.         0.         0.
0.         0.
(  rads(c )/source particle (neutrons)*10^-17 )
1.216      1.186      1.131      1.167      1.156      1.182      1.100
1.130      1.549      0.979      1.506      0.693      1.055      1.068
1.442      2.472      2.212      1.830      1.954      2.180      2.903
3.643      4.794      4.844      5.019      5.313      5.121      4.906
5.018      5.196      4.370      4.841      4.674      5.090      6.606
12.08      109.3      0.         0.         0.         0.         0.
0.         0.         0.         0.         0.         0.         0.
0.         0.         0.         0.         0.         0.         0.
0.         0.
(  rads(si)/source particle (neutrons)*10^-17 )
10.47      11.19      11.56      11.6       11.39      11.08      10.62
9.983      9.229      9.239      10.02      6.831      3.770      3.771
3.230      2.990      3.706      3.532      4.579      4.435      5.999
```

```
8.903     1.331     3.428     3.190     3.387     3.661     4.367
4.585     4.778     4.217     7.061     19.84     81.82     448.8
1994.0    30540.0   0.        0.        0.        0.        0.
0.        0.        0.        0.        0.        0.        0.
0.        0.        0.        0.        0.        0.        0.
0.        0.
(eV/CM^2/SOURCE PARTICLE xrays )
0.        0.        0.        0.        0.        0.        0.
0.        0.        0.        0.        0.        0.        0.
0.        0.        0.        0.        0.        0.        0.
0.        0.        0.        0.        0.        0.        0.
0.        0.        0.        0.        0.        0.        0.
0.        0.        1.        1.        1.        1.        1.
1.        1.        1.        1.        1.        1.        1.
1.        1.        1.        1.        1.        1.        1.
1.        1.
(  rads(c )/source particle (xrays)*10^-17  )
0.        0.        0.        0.        0.        0.        0.
0.        0.        0.        0.        0.        0.        0.
0.        0.        0.        0.        0.        0.        0.
0.        0.        0.        0.        0.        0.        0.
0.        0.        0.        0.        0.        0.        0.
0.        0.        2.190     2.331     2.435     2.540     2.682
2.870     3.126     3.392     3.624     3.914     4.267     4.581
4.733     4.698     4.369     3.698     3.390     3.453     10.43
16.35     92.77
(  rads(si)/source particle (xrays)*10^-17  )
0.        0.        0.        0.        0.        0.        0.
0.        0.        0.        0.        0.        0.        0.
0.        0.        0.        0.        0.        0.        0.
0.        0.        0.        0.        0.        0.        0.
0.        0.        0.        0.        0.        0.        0.
0.        0.        30.12     29.76     29.64     29.91     30.56
31.52     33.01     34.85     36.69     39.22     42.59     45.74
47.40     47.53     46.92     55.79     92.25     241.9     924.2
3305.0    17630.0
(eV/CM^2/EV/SOURCE PARTICLE )
    4    5    6    7    8    9   10   11   12   13   14   15   16   17
   18   19   20   21   22   23   24   25   26   27   28   29   30   31
   32   33   34   35   36   37   38   39   40   41   42   43   44   45
   46   47   48   49   50   51   52   53   54   55   56   57   58
(eV/CM^2/SEC/SOURCE PARTICLE det 1   rads/sec/source particle det 2)
(eV/CM^2/EV/SEC/SOURCE PARTICLE)
.000000001.000000005.000000006.000000007.000000008.000000009.00000001
.000000011.000000012.000000013.000000014.000000015.000000016.000000018
.000000019.00000002 .000000021.000000022.000000023.000000024.000000025
.000000026.000000027.000000028.000000029.000000030.000000031.000000032
.000000033.000000034.000000035.000000036.000000037.000000038.000000039
.00000004 .00000005 .000000075.0000001  .000001   .00001    .0001
.001      .005      .01       .1        1.0
$$$$$$$$$$$$$$ LMF-RV PROBLEM. DON NICHOLS Aug 88 $$$$$$$$$$$$$$$
```

REFERENCES

1. Bridgman, Charles J. The Physics and Effects of Nuclear Explosives, Class Notes, Air Force Institute of Technology, Wright-Patterson AFB OH, 1988.

2. Messenger, G. C. and M. S. Ash. The Effects of Radiation on Electronic Systems, Van Nostrand Reinhold Co., New York, 1986.

3. Glasstone, Samuel and Phillip J. Dolan. The Effects of Nuclear Weapons (Third Edition), U.S. Department of Defense, Washington D.C., 1977.

4. Hogan, William J. A MULTIUSER DEVELOPMENT SCENARIO FOR ICF, UCRL-93568, Seventh International Workshop on Laser Interaction and Related Plasma Phenomena, Monterey, CA, October 1985.

5. Emmit, M.B. The MORSE Monte Carlo Radiation Transport Code System, ORNL-4972/R2, Oak Ridge National Laboratory, Oak Ridge, Tenn, July 1984.

6. Chen, Francis F. Introduction to Plasma Physics and Controlled Fusion (Second Edition), Plenum Press, New York, 1984.

7. Friedlander, Gerhart et al. Nuclear and Radiochemistry (Third Edition), John Wiley and Sons, New York, 1981.

8. Bartine, D.E. et al. Production and Testing of the DNA Few-Group Coupled Neutron-Gamma Cross-Section Library, ORNL/TM-4840, Oak Ridge National Laboratory, Oak Ridge, Tenn, March 1977.

9. Dolan, Thomas James. Fusion Research, Vol II, Experiments, Pergamon Press, New York, 1982.

REPORT DOCUMENTATION PAGE

Form Approved
OMB No. 0704-0188

1a. REPORT SECURITY CLASSIFICATION UNCLASSIFIED	1b. RESTRICTIVE MARKINGS
2a. SECURITY CLASSIFICATION AUTHORITY	3. DISTRIBUTION/AVAILABILITY OF REPORT Approved for public release; distribution unlimited.
2b. DECLASSIFICATION/DOWNGRADING SCHEDULE	
4. PERFORMING ORGANIZATION REPORT NUMBER(S) AFIT/GNE/ENP/89M-6	5. MONITORING ORGANIZATION REPORT NUMBER(S)
6a. NAME OF PERFORMING ORGANIZATION School of Engineering 6b. OFFICE SYMBOL (If applicable) AFIT/ENP	7a. NAME OF MONITORING ORGANIZATION
6c. ADDRESS (City, State, and ZIP Code) Air Force Institute of Technology (AU) Wright-Patterson AFB OH 45433-6583	7b. ADDRESS (City, State, and ZIP Code)
8a. NAME OF FUNDING/SPONSORING ORGANIZATION 8b. OFFICE SYMBOL (If applicable)	9. PROCUREMENT INSTRUMENT IDENTIFICATION NUMBER
8c. ADDRESS (City, State, and ZIP Code)	10. SOURCE OF FUNDING NUMBERS PROGRAM ELEMENT NO. / PROJECT NO. / TASK NO. / WORK UNIT ACCESSION NO.
11. TITLE (Include Security Classification) see block 19	
12. PERSONAL AUTHOR(S) Don F. Nichols, B.S., 2d Lt, USAF	
13a. TYPE OF REPORT MS Thesis 13b. TIME COVERED FROM _____ TO _____	14. DATE OF REPORT (Year, Month, Day) 1989 March 15. PAGE COUNT 92
16. SUPPLEMENTARY NOTATION	

17. COSATI CODES		
FIELD	GROUP	SUB-GROUP
19	11	

18. SUBJECT TERMS (Continue on reverse if necessary and identify by block number)
Hard X Rays, Weapons Effects, Simulators, Inertial Confinement Fusion, ICF, Laboratory Microfusion Facility

19. ABSTRACT (Continue on reverse if necessary and identify by block number)

Title: SPECTRAL AND TEMPORAL FIDELITY OF A HARD X-RAY WEAPONS EFFECTS SIMULATION TEST IN A HIGH-GAIN ICF FACILITY

Thesis Chairman: Denis E. Beller, Major, USAF
Assistant Professor of Engineering Physics

(Abstract on reverse)

20. DISTRIBUTION/AVAILABILITY OF ABSTRACT ☒ UNCLASSIFIED/UNLIMITED ☐ SAME AS RPT. ☐ DTIC USERS	21. ABSTRACT SECURITY CLASSIFICATION UNCLASSIFIED
22a. NAME OF RESPONSIBLE INDIVIDUAL Denis E. Beller, Major, USAF	22b. TELEPHONE (Include Area Code) (513) 255-4498 22c. OFFICE SYMBOL AFIT/ENP

ABSTRACT (continued from Block 19)

The MORSE-CG Monte Carlo code was used to examine the feasibility of using the proposed Laboratory Microfusion Facility (LMF) to simulate the effects of hard X rays from a nuclear weapon. The LMF will be an inertial confinement fusion facility for the testing of high-gain deuterium-tritium (DT) pellets, and will produce a pulse of hard X rays and neutrons over a very short time interval. A spherical shell of ^{6}LiH with a thickness of 60 cm was found to spread an instantaneous 10 keV X-ray pulse temporally over a period of 16 ns. The peak of the X-ray spectrum shifted down in energy from the 37.5 keV peak of the input spectrum to a final energy of 25 keV. Eighty-seven percent of the source X-ray intensity was lost to the LiH, resulting in a final fluence of 10.8 cal/cm^2 and a final dose of 9.3 Mrads(Si) 250 cm from the source. Fifty percent of the X-ray dose arrived during an interval of 6 ns, giving a dose rate of $8*10^{14}$ rads(Si)/sec. The only serious problem with the use of the LMF for hard X-ray simulation was the fluence of one-MeV-equivalent neutrons. The minimum fluence achieved was on the order of $1*10^{14}$ n/cm^2, but preliminary work has indicated that this value could be reduced by an appropriate shadow shield, and that the LMF may be a viable candidate for hard X-ray weapons effects work.